Neurotoxicology 71 (2019) 60–74

Contents lists available at ScienceDirect

Neurotoxicology

journal homepage: www.elsevier.com/locate/neuro

Full Length Article

Phosphorylation of extracellular signal-regulated kinase 1/2 in subepidermal nerve fibers mediates hyperalgesia following diabetic peripheral neuropathy

Chiung-Hui Liu[a,b], Chyn-Tair Lan[a,b], Li-You Chen[a,b], Wen-Chieh Liao[a,b], Miau-Hwa Ko[c], To-Jung Tseng[a,b,*]

[a] Department of Anatomy, Institute of Medicine, Chung Shan Medical University, Taichung 40201, Taiwan
[b] Department of Medical Education, Chung Shan Medical University Hospital, Taichung 40201, Taiwan
[c] Department of Anatomy, College of Medicine, China Medical University, Taichung 40402, Taiwan

ARTICLE INFO

Keywords:
Streptozotocin
Hypersensitivity
Subepidermal nerve fibers
Neuropeptides
Extracellular signal-regulated kinase 1/2
Transient receptor potential vanilloid channels.

ABSTRACT

Peripheral neuropathy, a chronic complication of diabetes mellitus (DM), is often accompanied by the onset of severe pain symptoms that affect quality of life. However, the underlying mechanisms remain elusive. In the present study, we used Sprague–Dawley rats to establish a rodent model of the human type 1 DM by a single intraperitoneal (i.p.) injection with streptozotocin (STZ) (60 mg/kg). Hypersensitivity, including hyperalgesia and allodynia, developed in the STZ-induced diabetic rats. Cutaneous innervation exhibited STZ-induced reductions of protein gene product 9.5-, peripherin-, and neurofilament 200-immunoreactivity (IR) subepidermal nerve fibers (SENFs). Moreover, the decreases of substance P (SP)- and calcitonin gene-related peptide (CGRP)-IR SENFs were distinct gathered from the results of extracellular signal-regulated kinase 1 and 2 (ERK1/2)- and phosphorylated ERK1/2 (pERK1/2)-IR SENFs in STZ-induced diabetic rats. Double immunofluorescence studies demonstrated that STZ-induced pERK1/2-IR was largely increased in SENFs where only a small portion was colocalized with SP- or CGRP-IR. By an intraplantar (i. pl.) injection with a MEK inhibitor, U0126 (1,4-Diamino-2,3-dicyano-1,4-bis[2-aminophenylthio]butadiene), hyperalgesia was attenuated in a dose-responsive manner. Botulinum toxin serotype A had dose-dependent analgesic effects on STZ-induced hyperalgesia and allodynia, which exhibited equivalent results as the efficacy of transient receptor potential vanilloid (TRPV) channel antagonists. Morphological evidence further confirmed that STZ-induced SP-, CGRP- and pERK1/2-IR were reduced in SENFs after pharmacological interventions. From the results obtained in this study, it is suggested that increases of pERK1/2 in SENFs may participate in the modulation of TRPV channel-mediated neurogenic inflammation that triggers hyperalgesia in STZ-induced diabetic rats. Therefore, ERK1/2 provides a potential therapeutic target and efficient pharmacological strategies to address hyperglycemia-induced neurotoxicity.

1. Introduction

Clinically, the human type 1 diabetes mellitus (DM) occurs when pancreatic beta cells are destroyed, and adequate insulin is not produced in the islets of Langerhans (Mathis et al., 2001; Tripathi and Srivastava, 2006). The disturbance of glucose metabolism in the human type 1 DM causes acute hyperglycemia and may result in severe chronic complications, including retinopathy, neuropathy, and nephropathy (Todorovic, 2016; Tripathi and Srivastava, 2006). Peripheral neuropathy occurs in 50%–70% of the human type 1 DM, presenting as nociceptive dysfunction in a distal symmetrical stocking-and-glove distribution (Todorovic, 2016; Obrosova, 2009). Several pain symptoms, characterized by paresthesia, hypersensitivity, and spontaneous pain, have a major influence on the quality of life (Todorovic, 2016). Hypersensitivity is defined as an increase of responsive sensitivity to noxious stimuli (hyperalgesia) and innocuous stimuli (allodynia), which are used to assess the pain symptoms in the human type 1 DM (Todorovic, 2016; Tripathi and Srivastava, 2006).

Abbreviations: DM, diabetes mellitus; STZ, streptozotocin; SENFs, subepidermal nerve fibers; IR, immunoreactivity; PGP9.5, protein gene product 9.5; NF200, neurofilament 200; SP, substance P; CGRP, calcitonin gene-related peptide; ERK1/2, extracellular signal-regulated kinase 1 and 2; i.pl., intraplantar; BoNT/A, Botulinum toxin serotype A; TRPV, transient receptor potential vanilloid; PIW, post-induction week; PID, post-injection day; PIH, post-injection hour

* Corresponding author at: Department of Anatomy, School of Medicine, Chung Shan Medical University, No. 110, Jian-Guo N. R., Sec. 1, Taichung 40201, Taiwan.
E-mail address: tjtseng@csmu.edu.tw (T.-J. Tseng).

https://doi.org/10.1016/j.neuro.2018.12.006
Received 9 October 2018; Received in revised form 18 December 2018; Accepted 21 December 2018
Available online 21 December 2018
0161-813X/

Traditional diagnostic methodology depends on a histological examination of tissue from a sural nerve biopsy (Myers et al., 2013; Polydefkis et al., 2001). Nerve degeneration, paranodal demyelination, Schwann cell abnormality, and endoneural microangiopathy are described as obvious pathological evidence in the human type 1 DM (Obrosova, 2009; Callaghan et al., 2012; Giannini and Dyck, 1994). Moreover, human skin biopsy, a minimally invasive procedure, is used to estimate the integrity of cutaneous innervation with protein gene product 9.5 (PGP9.5) by immunohistochemistry (Polydefkis et al., 2001; Chien et al., 2001). In the human type 1 DM, the quantitation of density of intraepidermal nerve fibers (IENFs) is used to demonstrate the progressive processes of nerve degeneration in epidermis (Umapathi et al., 2007; Kennedy et al., 1996; Hirai et al., 2000). Importantly, a significant loss of IENFs elucidates the correlative symptoms of hyposensitivity, such as thermal hypoalgesia and mechanical hypoalgesia, in long-term human type 1 DM (Hirai et al., 2000). Recently, several clinical studies about painful peripheral neuropathy have used skin biopsies to focus on primary afferents in dermis that are described as subepidermal nerve fibers (SENFs) (Myers et al., 2013; Provitera et al., 2007). Hence, the quantitation of areas of SENFs may provide a novel way to define the different phenotypes of primary afferents, especially in the human type 1 DM.

Neuropeptides, such as substance P (SP) and calcitonin gene-related peptide (CGRP), modulated by calcium influx through the transient receptor potential vanilloid (TRPV) 1 channel, are released from primary afferents in the skin (Gouin et al., 2017; Devesa et al., 2014). SP and CGRP facilitate an increase in vasodilation and vascular permeability, causing tissue edema. Also, SP stimulates the degranulation of mast cells and local infiltration of leukocytes (Gouin et al., 2017; Pinho-Ribeiro et al., 2017). These increased immune cells in the skin release pro-inflammatory cytokines, *i.e.*, tumor necrosis factor alpha, interleukin, and interferon, which lead to nerve terminal swelling and myelin extirpation like that detected in the early stages of Wallerian degeneration (Zhang et al., 2017; Wang and Lehky, 2012). This progressive pathophysiologial process in the skin is in response to the release of neuropeptides from primary afferents, which is described as neurogenic inflammation (Choi and Di Nardo, 2018; Pinho-Ribeiro et al., 2017).

Mitogen-activated protein kinases (MAPKs) are the end-stage downstream kinases of a cascade initiated with the activation of Ras family by the phosphorylation of receptor tyrosine kinase (Johnson and Lapadat, 2002; Aley et al., 2001; Wood et al., 1992). The well-defined subfamilies of MAPKs, including the extracellular signal-regulated kinase 1/2 (ERK1/2), c-Jun N-terminal kinase (JNK), and p38 kinase, are related to axonal guidance, dendritic arborization, and neuronal differentiation (Johnson and Lapadat, 2002; Purves et al., 2001). Early clinical manifestations in the human type 1 DM show the phosphorylation of ERK1/2 in the sural nerve is significantly higher than the phosphorylation of JNK or p38 kinase through immunoblotting (Purves et al., 2001). However, the linkage of phosphorylation of ERK1/2 to the human type 1 DM is not supported by the results in streptozotocin (STZ)-induced diabetic rats that only exhibit the phosphorylation of ERK1/2 in the dorsal root ganglia (DRG) (Purves et al., 2001; Ji et al., 1999).

Sprague–Dawley rats were given a single intraperitoneal (i.p.) injection with STZ, which was principally used as a cytotoxic agent for destroying pancreatic beta cells, for establishing an animal model of human type 1 DM (Calcutt, 2004). The purpose of the present study in STZ-induced diabetic rats was to 1) evaluate the temporal changes of metabolic parameters and hypersensitivity; 2) clarify the alterations of SENFs, including the different phenotypes of primary afferents; 3) interpret the changes of peptidergic SENFs and the local effects of Botulinum toxin serotype A (BoNT/A); 4) elucidate the expression of ERK1/2 and phosphorylated ERK1/2 (pERK1/2) in SENFs and its peripheral role through pharmacological intervention with U0126; and 5) prove the potential processes of neurogenic inflammation by studying the effects of TRPV channel antagonists on hypersensitivity.

2. Materials and methods

2.1. Human Type 1 diabetes mellitus in rats

Adult male Sprague–Dawley rats (200–250 g), weighing 200 ~ 250 g, were divided into two experimental groups: the STZ group, which was induced by a single i.p. STZ (pH 4.0, 60 mg/kg, n = 24) induction; and the Citrate group, i.p. injected with a control citrate solution (pH 4.0, n = 16). All rats were housed in plastic cages with soft sawdust as bedding to avoid mechanical damage to the footpad. All procedures were conducted in accordance with the ethical guidelines set up by the International Association for the Study of Pain (IASP) on the use of laboratory animals in experimental research, and the study protocol was approved by the Animal Committee of Chung Shan Medical University, Faculty of Medicine, Taichung, Taiwan (IASP Committee, 1980).

2.2. Experimental design

All rats from the STZ group and from the Citrate group were monitored the metabolic parameters, containing blood glucose levels, HbA1c levels and body weights every 2 weeks. Blood glucose level was tested by a one-touch glucose meter (Johnson & Johnson, US) and HbA1c level was measured using the Test Kit Glyco-Tek Affinity Column Method (Helena Laboratories, Beaumont, TX) (Lin et al., 2008). Behavioral assessments were evaluated at the following time points: post-induction week (PIW) 0 (designated as the pretest baseline data), PIW 2, PIW 4, PIW 6, and PIW 8. Then, all rats were sacrificed periodically at PIW 2, PIW 4, PIW 6, and PIW 8.

2.3. Behavior assessments

Thermal hyperalgesia was estimated by measuring withdrawal latency upon the stimulation of radiant heat using a Hargreaves-type analgesiometer (Ugo Basile, Comerio-Varese, Italy) with a radiant heat source (a halogen projector lamp, 50 W, 8 V) (Ko et al., 2016). Mechanical hyperalgesia was evaluated by the noxious pinprick stimulation (A Von Frey–type 0.5 mm filament) with Dynamic Plantar Aesthesiometer (Code: 37450, Ugo Basile, Comerio-Varese, Italy) and recorded as withdrawal threshold (Samur et al., 2018). Mechanical allodynia was determined by measuring mechanical threshold depended on a withdrawal response according to an up-and-down method using a series of calibrated Von Frey monofilaments (Senselab aesthesiometer, Somedic Sales AB, Stockholm, Sweden) (Ko et al., 2016).

2.4. Immunohistochemistry

Animal tissue was prepared as previous report (Ko et al., 2015). Briefly, the sections were quenched with 1% H_2O_2 in methanol, blocked with 5% normal goat serum in 0.5% nonfat dry milk/Tris, then incubated with the following primary antisera overnight respectively: (1) rabbit polyclonal protein gene product 9.5 (PGP9.5, 1: 1000, UltraClone, Isle of Wight, UK); (2) rabbit polyclonal peripherin (1:1000, Millipore, Billerica, MA); (3) rabbit polyclonal neurofilament 200 (NF200, 1:1000, Sigma Chemicals, St. Louis, MO); (4) rabbit polyclonal substance P (SP, 1:1000, Immunostar, Hudson, WI); (5) rabbit polyclonal calcitonin gene-related peptide (CGRP, 1:1000, Millipore, Billerica, MA); (6) rabbit polyclonal phospho-extracellular signal-regulated kinase 1/2 (pERK1/2, 1:1000, Cell Signaling Technology, Beverly, MA); (7) rabbit polyclonal ERK1/2 (1:1000, Cell Signaling Technology, Beverly, MA) at 4 °C overnight, respectively. Avidin-biotin complex kit (Vector Laboratories, Burlingame, CA) was used. The specific immunostaining was visualized with 3,3′-diaminobenzidine (DAB, Sigma Chemicals, St. Louis, MO).

2.5. Quantitation of SENFs areas

The standard procedure for measuring SENFs area was carried out according to a protocol published in our previous study (Ko et al., 2016). In Brief, high-definition monochrome images were photographed under an Olympus microscope (BH2; Olympus, Tokyo, Japan) with a digital camera at a magnification of 100 × . Dermal area was therefore defined as an area within a width of 2.5 mm in epidermal length and at a depth of 200 μm below the dermal-epidermal junction. All the areas of interest were edited by Magic Wand Tool depending on individual antiserum tolerance to eliminate noises from background staining (the collagen fibers of the dermis) and calculated with Adobe Photoshop Elements 9.0 (Adobe Systems, San Jose, CA, USA). The area of interest was measured in pixels then transformed to μm^2 according to the relationships between pixel size and magnification. Every fourth section was quantified and the mean of these four SENFs areas was defined as the SENFs area of that rat.

2.6. Double immunofluorescence study

The sections from the STZ group at PIW 2 were processed for double immunofluorescent staining. In brief, the sections were blocked with 5% normal goat serum with 0.5% Triton X-100 in 0.5 M Tris for 1 h at room temperature. A combination of primary antisera, including (1) rabbit polyclonal pERK1/2 (1:100, Cell Signaling Technology, Beverly, MA) and mouse monoclonal SP (1:100, Santa Cruz Biotechnology; Santa Cruz, CA); (2) rabbit polyclonal pERK1/2 (1:100, Cell Signaling Technology, Beverly, MA) and mouse monoclonal CGRP (1:100, Santa Cruz Biotechnology; Santa Cruz, CA); (3) rabbit polyclonal CGRP (1:100, Millipore, Billerica, MA) and mouse monoclonal SP (1:100, Santa Cruz Biotechnology; Santa Cruz, CA), was prepared to incubate overnight at 4 °C, respectively. After rinsing in Tris, the sections were incubated with a mixture of secondary antibodies, *i.e.* (1) Alexa Fluor® 488-conjugated anti-rabbit IgG and (2) Alexa Fluor® 594-conjugated anti-mouse IgG (both from Invitrogen, Carlsbad, CA) for another hour. The sections were photographed under a conventional epifluorescent microscope (Zeiss Axiophot, Carl Zeiss, Heidelberg, Germany) equipped with appropriate filters. The standard quantitation of SENFs areas was setup and modified from the previous protocol.

2.7. Pharmacological interventions

2.7.1. BoNT/A

BoNT/A (BOTOX®, Allergan Corp, Irvine, CA) was reconstituted in adequate volume of 0.9% saline to set up four different final concentrations of vehicle, 3U/kg, 5U/kg, and 7U/kg respectively. Pharmacological agents were administered by an intraplantar (i.pl.) injection using the same protocol (Ko et al., 2015). Briefly, under ether anesthesia, a 26-gauge needle connected to a 10 μL Hamilton syringe (model: 701; Hamilton Company, Reno, NV, USA) was subdermally inserted into the plantar aspect for about 30 s and then disinfected with 70% alcohol. In this assessment, the baseline values of hypersensitivity were established at PIW 2 after STZ induction, defined as the post-injection day (PID) 0. According to the concentrations of BoNT/A, STZ-induced diabetic rats were randomly separated into four groups (n = 4 per group). After an i.pl. injection, hypersensitivity was assessed at PID 1, PID 3, PID 7, and PID 14 in all rats. Based on our interests that whether effect of BoNT/A on the morphological changes of SENFs is occurred following STZ induction, we performed two groups of STZ-induced diabetic rats given with BoNT/A 7U/kg and vehicle by an i.pl. injection, and then sacrificed at PID 3 and PID 14 respectively (n = 4 per time point in each group).

2.7.2. U0126

U0126 was obtained from Tocris Bioscience (Ellisville, MO) and added to a vehicle solution (10% Dimethyl sulfoxide (DMSO)) to set up four different final concentrations of vehicle, 1 μM, 20 μM, and 50 μM respectively. U0124, an inactive analog of U0126, was obtained from Tocris Bioscience (Ellisville, MO) and final concentration of 50 μM in a vehicle solution was set up as a negative control. Pharmacological agents were administered by an i.pl. injection through an established protocol for the purpose of reducing inflammatory responses (Ko et al., 2015). In this evaluation, we first established the baseline values of STZ-induced hypersensitivity at PIW 2, defined as the post-injection hour (PIH) 0. Based on the concentrations of U0126 (vehicle, 1 μM, 20 μM, and 50 μM) and U0124 (50 μM), the rats after STZ induction were randomly separated into five groups (n = 4 per group). After an i.pl. injection, all rats were assessed every 1 h from 1 h to 6 h and 24 h (PIH 1 to PIH 6 and PIH 24) to evaluate hypersensitivity respectively. The rationale for the choice of such an order was in performing the least stressful measurement to first minimize the influence of the next measurement on the result and to avoid tissue damage. To recognize the effect of U0126 on the morphological changes of SENFs after STZ induction, we performed two groups of STZ-induced diabetic rats given with U0126 50 μM and vehicle by an i.pl. injection, and then sacrificed at PIH 6 (n = 4 per group).

2.7.3. TRPV channel antagonists

Capsazepin, a selective TRPV1 channel antagonist and TRPA1 channel agonist, was purchased from Sigma Aldrich (St. Louis, MO). RN-1734, a selective TRPV4 channel antagonist, was obtained from Tocris Bioscience (Bristol, UK). A vehicle solution was prepared with 1% DMSO (Sigma, St. Louis, MO) and 99% saline. Capsazepin was reconstituted in adequate volume of a vehicle solution to set up four individual final concentrations (vehicle, 1 mM, 5 mM, and 25 mM). Four different final concentrations of RN-1734 were also set up as vehicle, 30 mM, 60 mM, and 120 mM respectively. Pharmacological agents were administered by an i.pl. injection using the same protocol (Ko et al., 2015). In this assessment, the baseline values of STZ-induced hypersensitivity were established at PIW 2 and defined as the PIH 0. According to the concentrations of capsazepin (vehicle, 1 mM, 5 mM, and 25 mM) and RN-1734 (vehicle, 30 mM, 60 mM, and 120 mM), STZ-induced diabetic rats were randomly separated into four groups (n = 4 per group) in each TRPV channel antagonist treatment. After an i.pl. injection, all rats were assessed every 1 h from PIH 1 to PIH 6 and PIH 24 to evaluate hypersensitivity respectively. In order to compare the effects of different TRPV channel antagonists on the morphological changes of SENFs in STZ-induced diabetic rats, two groups in the TRPV1 channel antagonist treatment were given with vehicle and capsazepin 25 mM, and another two groups in the TRPV4 channel antagonist treatment were given with vehicle and RN-1734 120 mM by an i.pl. injection. All rats were then sacrificed at PIH 6 respectively (n = 4 each group). The standard quantitation of SENFs areas were measured according to the above protocol.

2.8. Statistical analysis

Examiners were blinded to the grouping information when performing all the laboratory procedures of measurement and quantitation. Values are expressed as mean ± standard deviation using GraphPad Prism (GraphPad, San Diego, CA, USA). Independent data from the metabolic parameters, behavioral assessments and morphological examinations were analyzed using Student's *t*-test. Statistical comparisons were made by a one-way repeated measures analysis of variance (ANOVA), followed by Bonferroni *post hoc* test, with the times as the within-subjects factor. Statistical comparisons were made by a two-way ANOVA, followed by Bonferroni *post hoc* test, with the concentrations of BoNT/A, U0126 and TRPV channel antagonists as between-subjects factors and time as the within-subjects factor. A probability value of less than 0.05 ($p < 0.05$) was considered statistically significant.

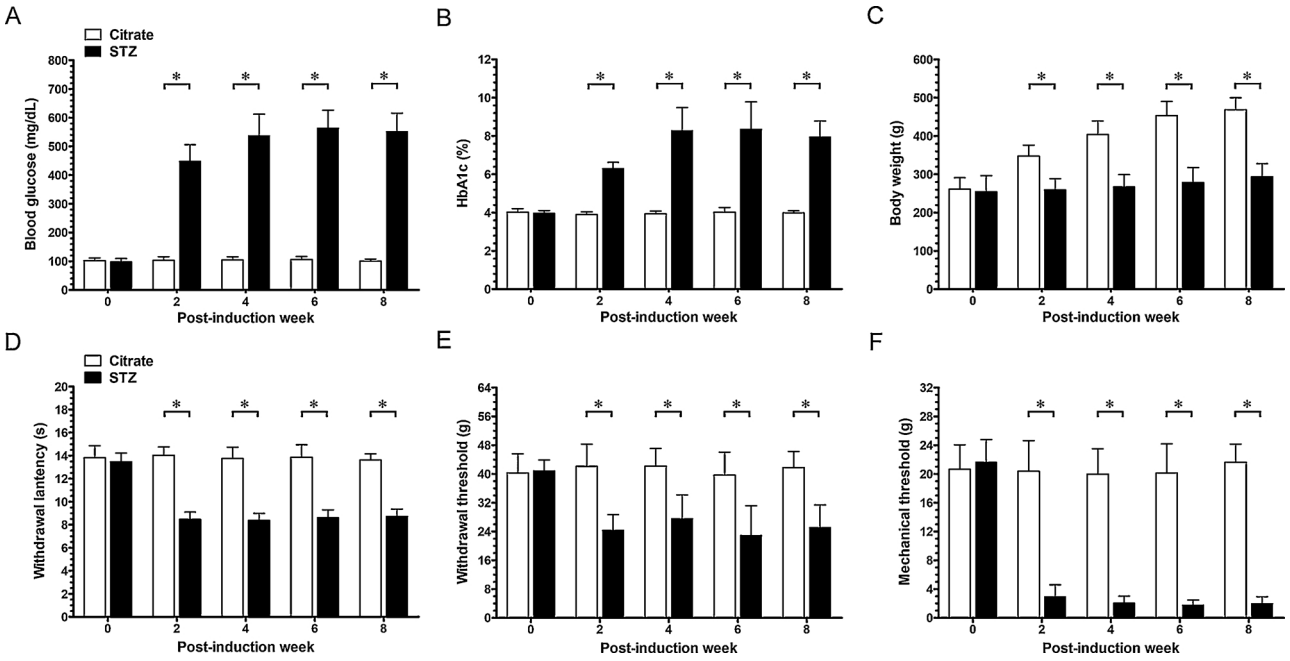

Fig. 1. Metabolic parameters and hypersensitivity after streptozotocin (STZ) induction. Graphs showed the temporal changes of (A) blood glucose levels, (B) hemoglobin A1c (HbA1c) levels, and (C) body weights, in the Citrate group (open bars) and the STZ group (filled bars). Temporal changes of hypersensitivity were shown in (D) thermal hyperalgesia, (E) mechanical hyperalgesia, and (F) mechanical allodynia. Thermal threshold of radial heat was defined as withdrawal latency (s) and the mechanical threshold of pinprick was demarcated as withdrawal threshold (g). The degree of mechanical allodynia was represented as mechanical threshold (g) in response to Von Frey monofilaments. All the measurements were expressed as the mean ± standard deviation (SD) (n = 4 in the Citrate group and n = 6 in the STZ group at each post-induction week (PIW)). Student's *t* test was applied to examine the differences against the values in the Citrate group at each time point. * $p < 0.05$ indicated as a significant difference. Statistical comparisons were made by a one-way repeated measures analysis of variance (ANOVA), followed by Bonferroni *post hoc* test, with the times as the within-subjects factor.

3. Results

3.1. Metabolic parameters following STZ induction in rats

To confirm the physiological manifestations in STZ-induced diabetic rats, glycemic control and body weight were compared between the STZ group and the Citrate group (Fig. 1). Two weeks after a single i.p. injection with STZ, the rats in the STZ group exhibited distinctive features of the human type 1 DM, including hyperglycemia (increased blood glucose levels) (> 400 mg/dl, Fig. 1A), elevated hemoglobin A1c (HbA1c) levels (> 6.0%, Fig. 1B), and slow gain of body weight (Fig. 1C), and increased water consumption beginning from PIW 2 to PIW 8 (*vs.* the Citrate group, $p < 0.05$, respectively). Rats in the Citrate group had normal blood glucose levels (< 120 mg/dl), normal HbA1c levels (< 6.0%), and normal body weight gain throughout the entire experiment.

3.2. STZ-induced hypersensitivity

The threshold of withdrawal response on the first footpad in rats was examined by radiant heat (thermal hyperalgesia), pinprick (mechanical hyperalgesia), and Von Frey monofilament (mechanical allodynia) (Fig. 1). Withdrawal latency ($p = 0.2320$) and withdrawal threshold ($p = 0.6304$) was comparable at PIW 0 (before STZ induction) for both groups (Fig. 1D and E). During the entire experimental period, withdrawal latency in the STZ group was consistently reduced (*vs.* the Citrate group, $p < 0.05$, respectively). The trend in mechanical hyperalgesia was like that in thermal hyperalgesia, with a decrease in withdrawal threshold from PIW 2 to PIW 8 in the STZ group (*vs.* the Citrate group, $p < 0.05$, respectively). Before STZ induction, mechanical thresholds were parallel between the groups ($p = 0.3378$) (Fig. 1F). From PIW 2 to PIW 8, the rats in the STZ group experienced a significant reduction in mechanical threshold (*vs.* the Citrate group, $p < 0.05$, respectively).

3.3. SENFs distributions following STZ induction

Immunostaining revealed morphological results with the antisera against PGP9.5, peripherin, and NF200, illuminating the changes in primary afferents in the dermis after STZ induction (Fig. 2). In the Citrate group, numerous PGP9.5-immunoreactivity (IR) SENFs aggregated into dermal nerve fascicles, ascending through the superficial dermis to form the subepidermal nerve plexus near the epidermal–dermal junction (Fig. 2A). In the STZ group, fragmented PGP9.5-IR SENFs with a degenerative appearance were definitively detected at PIW 2 (Fig. 2D). A similar degenerative pattern of PGP9.5-IR SENFs in the STZ group was still seen at PIW 8 (Fig. 2G). Based on these morphological results, temporal changes in the areas of PGP9.5-IR SENFs were verified by quantitation in both the STZ and Citrate group (Fig. 2J). Areas of PGP9.5-IR SENFs were reduced significantly in the STZ group at each time point (*vs.* the Citrate group, $p < 0.05$, respectively).

In the Citrate group, peripherin-IR SENFs, represented as unmyelinated C fibers and thinly myelinated Aδ fibers, mostly presented as dermal nerve fascicles and subepidermal nerve plexus adjacent to dermal papillae (Fig. 2B). In the STZ group, peripherin-IR SENFs were detected as swelling structures in nerve terminals, and expressional intensities declined at either PIW 2 or PIW 8 (Fig. 2E and 2 H). Areas of peripherin-IR SENFs showed a significant decrease in the STZ group until the end of experiments (Fig. 2K). In the Citrate group, NF200-IR SENFs, known as myelinated Aδ fibers and myelinated Aβ fibers, formed thick dermal nerve trunks and terminated horizontally close to epidermal–dermal junction (Fig. 2C). From PIW 2 to PIW 8, numerous NF200-IR SENFs in thick dermal nerve trunks gradually reduced in the STZ group, suggesting an obvious decrease of myelinated Aβ fibers (Fig. 2F and I). During the entire experimental period, areas of NF200-

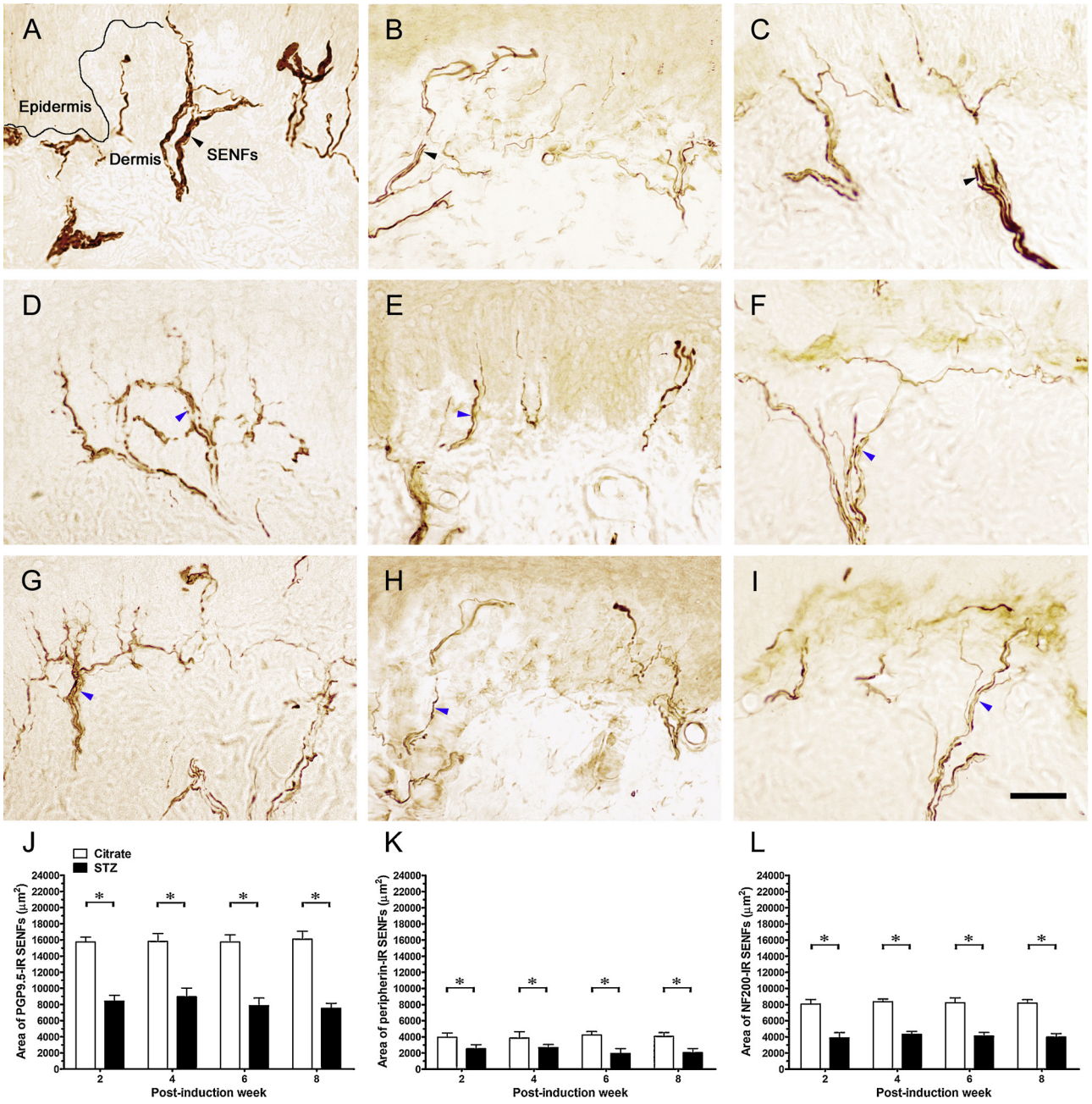

Fig. 2. Influences of STZ on subepidermal nerve fibers (SENFs) distribution. The sections were immunostained with the antisera against (A, D, G) protein gene product 9.5 (PGP9.5), (B, E, H) peripherin and (C, F, I) neurofilament 200 (NF200). (A, B, C) SENFs distributions in the Citrate group at PIW 2, and in the STZ group at (D, E, F) PIW 2 and (G, H, I) PIW 8 were displayed. (J, K, L) Panels showed the quantitative immunoreactivity (IR) SENFs areas. In the Citrate group, IR SENFs aggregated into dermal nerve fascicles (black arrowhead), ascended through superficial dermis to form subepidermal nerve plexus adjacent to the epidermal–dermal junction (black curved line in a). In the STZ group, these obvious degenerated signs of IR SENFs such as the nerve terminal swellings and fragmented profiles were frequently detected at PIW 2 and PIW 8 (blue arrowhead). Temporal changes of SENFs distribution in the Citrate group (open bars) and the STZ group (fill bars) were quantified by the results of IR, which were represented as the area of IR SENFs (mean ± SD; n = 4 in the Citrate group and n = 6 in the STZ group). Student's *t* test was applied to examine the differences against the values of the Citrate group at each time point. Statistical comparisons were made by a one-way ANOVA, followed by Bonferroni *post hoc* test, with the times as the within-subjects factor. Scale bar = 50 μm (For interpretation of the references to colour in this figure legend, the reader is referred to the web version of this article).

IR SENFs in the STZ group exhibited observable reductions, which were significantly different from those in the Citrate group (Fig. 2L).

3.4. Peptidergic SENFs distributions after STZ induction

The sections were immunostained with the antisera against SP and CGRP, and quantitative areas of SENFs were compared between the STZ group and the Citrate group (Fig. 3). In the Citrate group, SP-IR SENFs had a linear appearance, mainly in the subepidermal nerve plexus and perpendicularly toward dermal papillae (Fig. 3A). In the STZ group, withdrawal of SP-IR SENFs was observed in the subepidermal nerve plexus, presenting beaded shapes close to the epidermal–dermal junction on PIW 2 (Fig. 3C) that paralleled those observed on PIW 8 (Fig. 3E). Significant differences between the STZ and Citrate group in SP-IR SENFs areas were observed during the experimental period ($p < 0.05$, respectively) (Fig. 3G). In the Citrate group, CGRP-IR SENFs

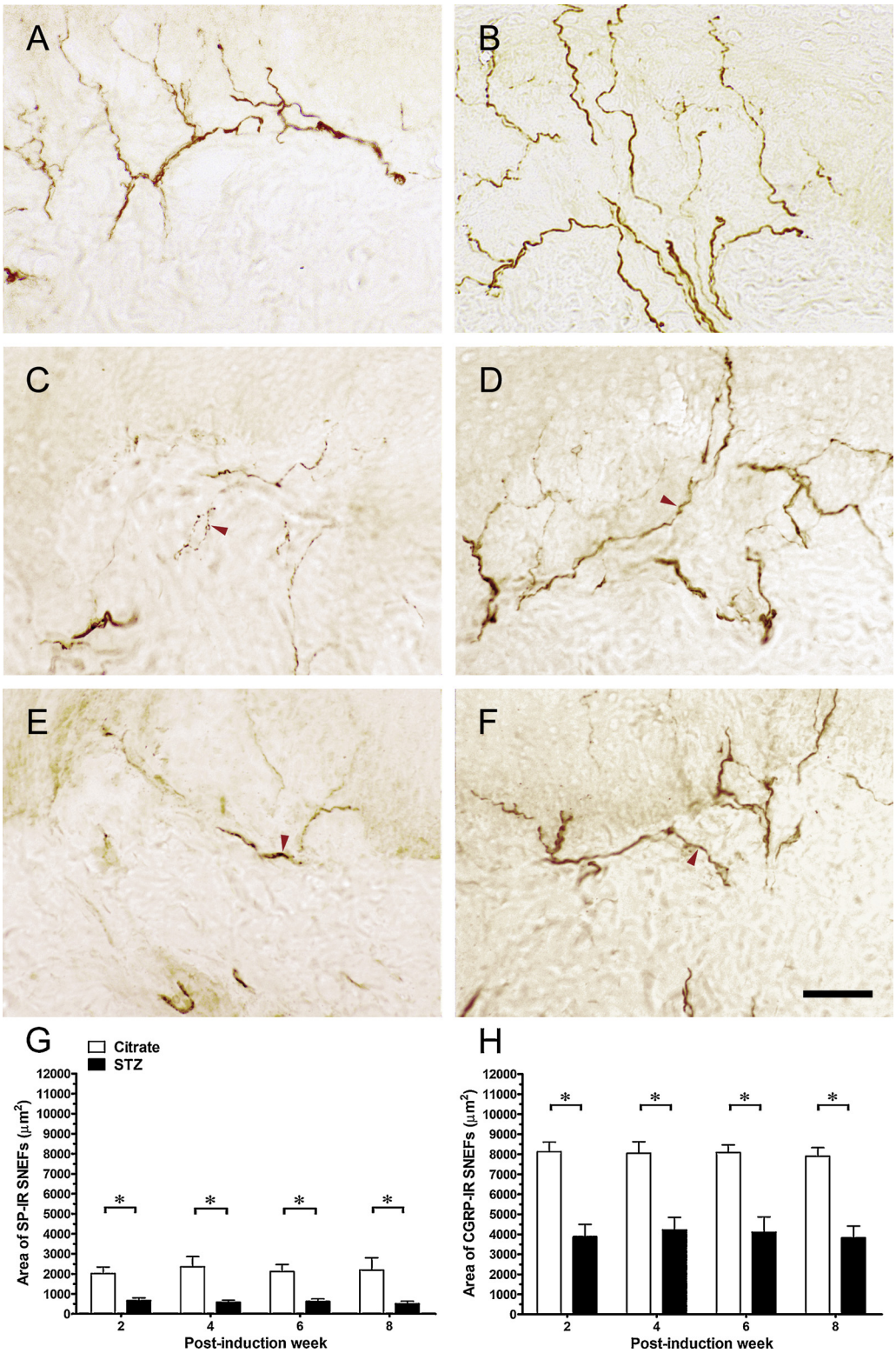

Fig. 3. STZ-induced changes of peptidergic SENFs distribution. The sections were immunostained with the antisera against (A, C, E) substance P (SP) and (B, D, F) calcitonin gene-related peptide (CGRP). Graphs showed (A, B) SENFs distributions in the Citrate group, and in the STZ group at (C, D) PIW 2 and (E, F) PIW 8. (G, H) Panels showed the quantitative peptidergic SENFs areas. In the Citrate group, SP-IR SENFs revealed the linear appearances mainly in subepidermal nerve plexus and towards dermal papillae perpendicularly. CGRP-IR SENFs starting from dermal nerve fascicles displayed irregular profiles towards epidermal-dermal junction and formed subepidermal nerve plexus In the STZ group, beaded varicosities and discontinuous fragments expressed in peptidergic SENFs were presented as noticeable degeneration signs (red arrowhead). The time-dependent changes of SENFs distribution in the Citrate group (open bars) and the STZ group (fill bars) were quantified by the results of IR, which were represented as the area of IR SENFs (mean ± SD; n = 4 in the Citrate group and n = 6 in the STZ group). Student's *t* test was applied to examine the differences against the values of the Citrate group at each time point. Statistical comparisons were made by a one-way ANOVA, followed by Bonferroni *post hoc* test, with the times as the within-subjects factor. Scale bar = 50 μm (For interpretation of the references to colour in this figure legend, the reader is referred to the web version of this article).

starting from dermal nerve fascicles displayed irregular profiles toward the epidermal–dermal junction and formed the subepidermal nerve plexus (Fig. 3B). At PIW 2, CGRP-IR SENFs in the STZ group extended from dermal nerve fascicles with discontinuous fragments observed near the superficial dermis (Fig. 3D). In addition, these fragmented forms of CGRP-IR SENFs were observed until PIW 8 (Fig. 3F). In the STZ group, areas of CGRP-IR SENFs were significantly reduced on PIW 2, and parallel depletions lasted until PIW 8 ($p < 0.05$, respectively) (Fig. 3H).

3.5. STZ-induced pERK1/2 and ERK1/2 expressions in SENFs

Changes in pERK1/2 and ERK1/2 expression in SENFs after STZ induction were examined by immunohistochemistry and the quantified areas of IR SENFs (Fig. 4). pERK1/2-IR SENFs in the Citrate group exhibited a linear appearance in dermal nerve fascicles with blunt rod-like

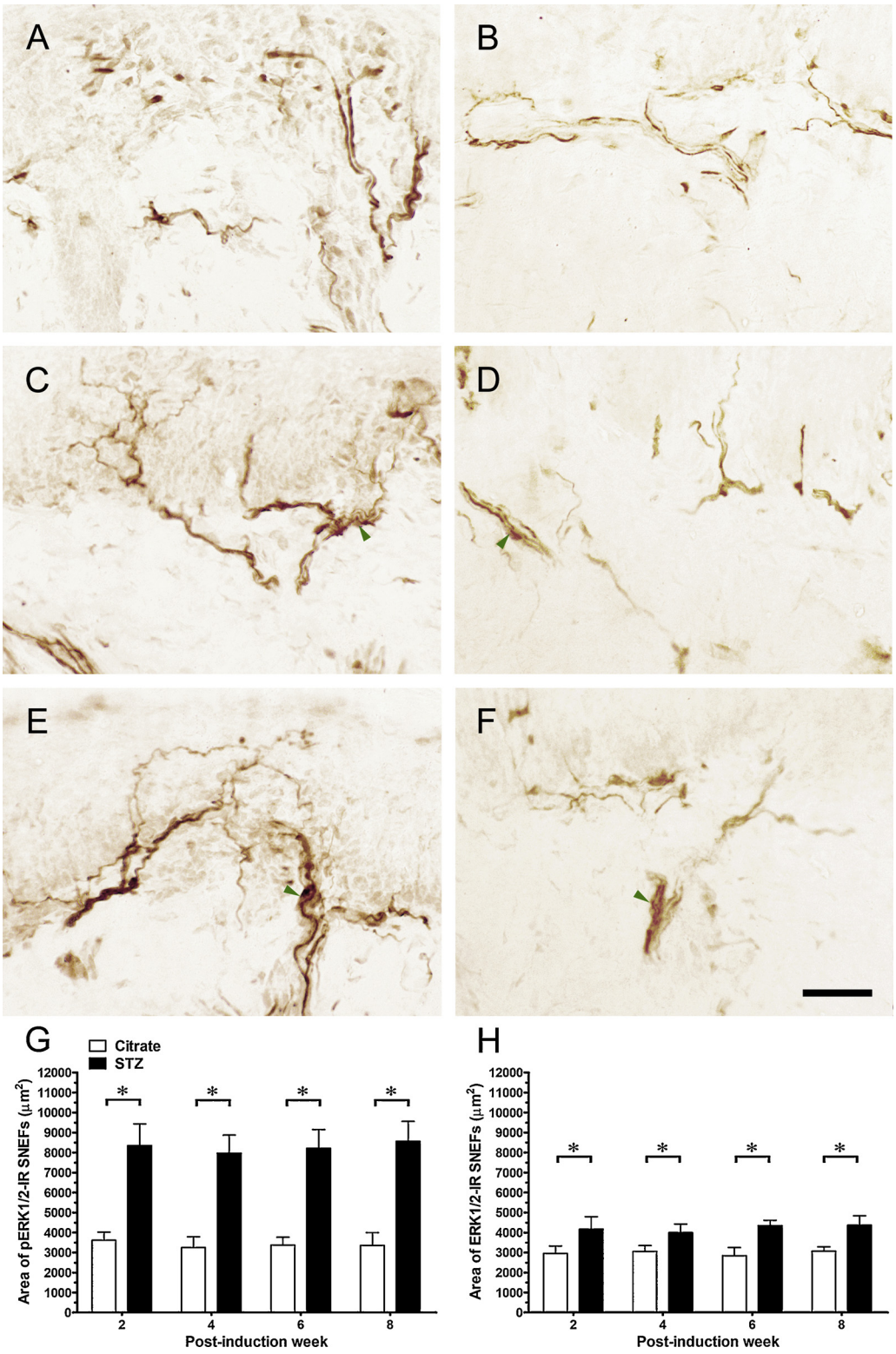

Fig. 4. Changes of phosphorylated extracellular signal-regulated kinase 1/2 (pERK1/2) and ERK1/2 expressions in SENFs after STZ induction. The sections were immunostained with the antisera against (A, C, E) pERK1/2 and (B, D, F) ERK1/2. (A, B) The IR of SENFs in the Citrate group, and the STZ group at (C, D) PIW 2 and (E, F) PIW 8 were exposed. (J, K, L) Panels showed the quantitative IR SENFs areas. IR SENFs in the Citrate exhibited linear appearances in the dermal nerve fascicles and with blunt rod-like nerve terminals adjacent epidermal-dermal junction. (C, E) pERK1/2-IR SENFs in the STZ group showed many linear shapes in dermal nerve fascicles and subepidermal nerve plexus formed numerous tiny sprouting nerve terminals. (D, F) In the STZ group, intensified ERK1/2-IR SENFs appeared to be seen in dermal nerve fascicles. The temporal changes of SENFs distribution in the Citrate group (open bars) and the STZ group (fill bars) were quantified by the results of IR, which were represented as the area of IR SENFs (mean ± SD; n = 4 in the Citrate group and n = 6 in the STZ group). Student's *t* test was applied to examine the differences against the values of the Citrate group at each time point. Statistical comparisons were made by a one-way ANOVA, followed by Bonferroni *post hoc* test, with the times as the within-subjects factor. Scale bar = 50 μm.

nerve terminals toward epidermal–dermal junction (Fig. 4A). Beginning on PIW 2, pERK1/2-IR SENFs in the STZ group showed many linear shapes in dermal nerve fascicles, and subepidermal nerve plexus formed numerous tiny sprouting nerve terminals (Fig. 4C). Through the entire experimental period, these similar forms of pERK1/2-IR SENFs in the STZ group were still clearly seen until PIW 8 (Fig. 4E). In the STZ group, these morphological results were used to measure increases in pERK1/2-IR SENFs area from PIW 2 to PIW 8 ($p < 0.05$, respectively) (Fig. 4G). ERK1/2-IR SENFs in the Citrate group were generally seen in the subepidermal nerve plexus around the epidermal–dermal junction (Fig. 4B). In the STZ group, the intensified ERK1/2-IR was observed in dermal nerve fascicles on either PIW 2 or PIW 8 (Fig. 4D and F). Quantitative comparisons of ERK1/2-IR SENFs areas showed a significant difference between the STZ and Citrate group during the entire experimental period ($p < 0.05$, respectively) (Fig. 4H).

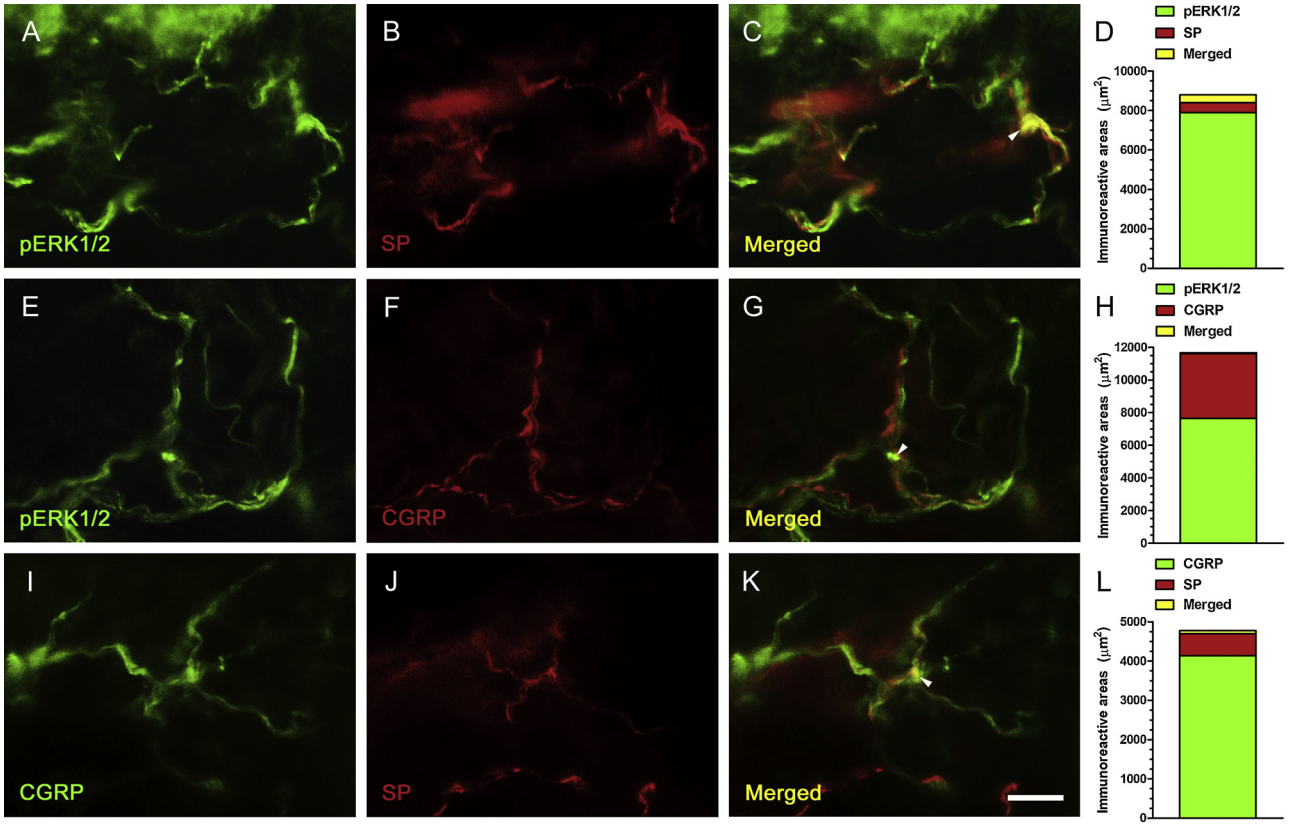

Fig. 5. Double immunofluorescence study of STZ-induced SENFs distribution. The sections from the STZ group at PIW 2 were immunostained with a combination of primary antisera, including (A, B) pERK1/2 and SP, (E, F) pERK1/2 and CGRP and (I, J) CGRP and SP. (A, E, I) Alexa Fluor® 488 (green) and (B, F, J) Alexa Fluor® 594 (red) were used to label IR in SENFs. (C, G, K) The merged images of IR SENFs illustrated colocalization in the superficial dermis of the skin. (D, H, L) Panels showed the quantitation of individual IR SENFs areas and their colocalized areas. Scale bar = 100 μm (For interpretation of the references to colour in this figure legend, the reader is referred to the web version of this article).

3.6. Colocalization of pERK1/2-IR SENFs and peptidergic SENFs after STZ induction

To elucidate relationships between the phosphorylation of ERK1/2 and neuropeptides in the primary afferents of the skin after STZ induction, the sections from the STZ group at PIW 2 were analyzed by double immunofluorescence (Fig. 5). pERK1/2-IR were predominantly colocalized with SP-IR in SENFs in subepidermal nerve plexus and tiny nerve terminals near the epidermal–dermal junction (Fig. 5A to 5C). Quantitative SENFs areas demonstrated that there were about 76.68% SP-IR SENFs colocalized with pERK1/2-IR SENFs (Fig. 5D). In contrast, although the distribution of pERK1/2-IR SENFs in dermal nerve fascicles was similar to CGRP-IR SENFs, pERK1/2 and CGPR were not meaningfully coexpressed (Fig. 5E to 5 G). Only 1.29% of CGRP-IR SENFs was colocalized with pERK1/2-IR SENFs (Fig. 5H). Moreover, CGRP-IR was colocalized with SP-IR in SENFs, which was mainly detected in the subepidermal nerve plexus (Fig. 5I–K). Quantitative SENFs areas revealed that approximately 13.52% SP-IR SENFs were colocalized with CGRP-IR SENFs (Fig. 5L).

3.7. Effects of BoNT/A on STZ-induced hypersensitivity

We hypothesized that peptidergic SENFs mediated STZ-induced hypersensitivity to initiate neurogenic inflammation. Thus, BoNT/A was used to block the release of neuropeptides from SENFs, and all hypersensitivity was assessed after i.pl. injection (Fig. 6). After STZ induction, the local effects of BoNT/A produced a dose-dependent ($F = 29.03$; $p < 0.0001$), significant increase of withdrawal latencies ($F = 2.67$; $p = 0.0062$) and changed the temporal pattern of thermal hyperalgesia ($F = 5.59$; $p = 0.0007$) (Fig. 6A). In the BoNT/A 7U/kg group, withdrawal latencies were rapidly increased and maintained from PID 1 to PID 7. On PID 14, withdrawal latencies had nearly returned to previous values. In the Vehicle group, STZ-induced diabetic rats exhibited comparable withdrawal latencies starting from PID 1 to PID 14 (*vs.* PID 0, $p > 0.05$, respectively).

BoNT/A slightly affected the increase of withdrawal thresholds ($F = 1.24$; $p = 0.2811$) in a dose-responsive manner ($F = 12.73$; $p < 0.0001$) and altered the pattern of mechanical hyperalgesia ($F = 3.85$; $p = 0.0075$) over time after STZ induction (Fig. 6B). In the BoNT/A 7U/kg group, withdrawal thresholds quickly increased and continued from PID 1 to PID 7; however, withdrawal thresholds had reverted on PID 14 and exhibited the trend of mechanical hyperalgesia. After STZ induction, the effects of BoNT/A on mechanical thresholds revealed a considerable increase ($F = 10.02$; $p < 0.0001$) dose-dependently ($F = 71.73$; $p < 0.0001$), and the time-based pattern of mechanical allodynia changed ($F = 22.54$; $p < 0.0001$) (Fig. 6C). For instance, STZ-induced mechanical thresholds in the BoNT/A 7U/kg group showed a significant reversal from PID 1 to PID 3 and partially returned on PID 14.

3.8. Influence of U0126 on hypersensitivity after STZ induction

To test the hypothesis that STZ-induced increases of pERK1/2-IR SENFs contributed to hypersensitivity, the role of U0126 after an i.pl. injection was investigated (Fig. 6). After STZ induction, the local effects of U0126 showed a significant increase of withdrawal latencies ($F = 14.18$; $p < 0.0001$) in a dose-responsive manner ($F = 269.8$; $p < 0.0001$) and changed the sequential pattern of thermal hyperalgesia ($F = 31.05$; $p < 0.0001$) (Fig. 6D). In the U0126 50 μM group, withdrawal latencies were rapidly intensified and sustained from PIH 1

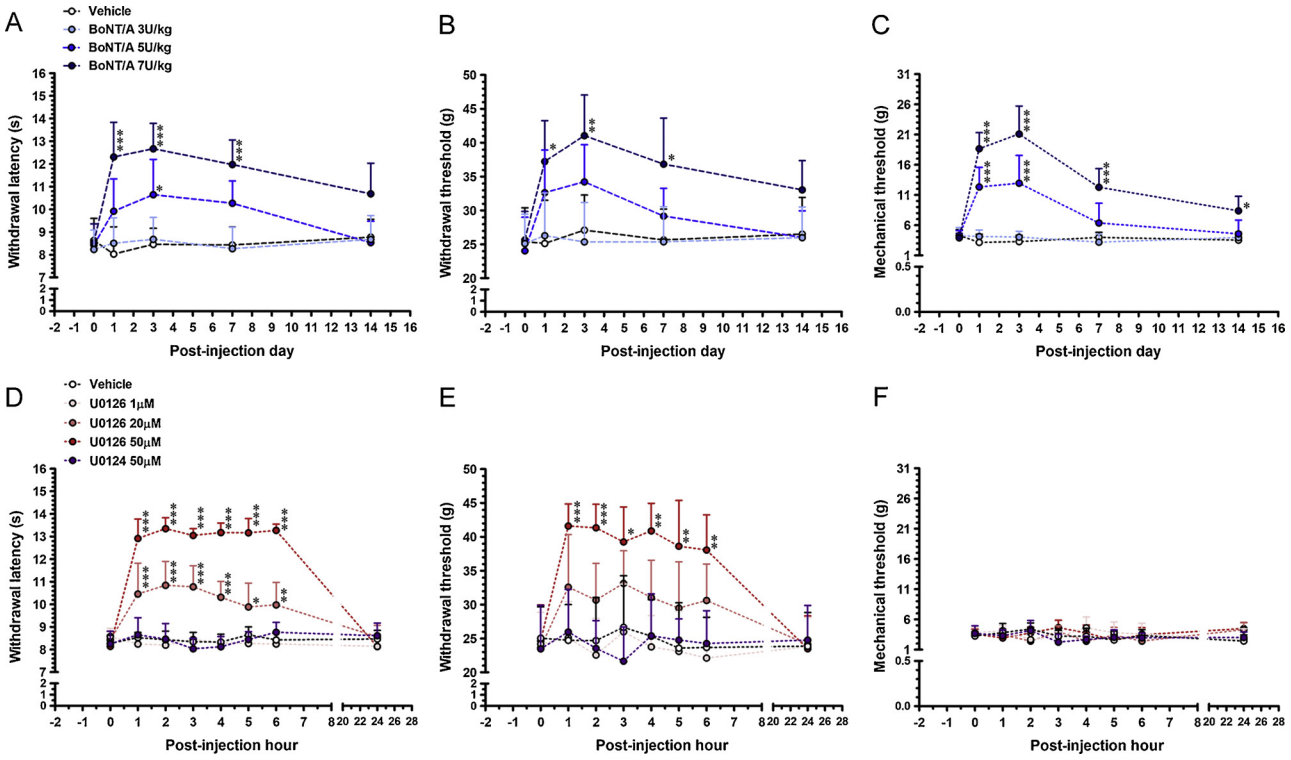

Fig. 6. Effects of Botulinum toxin type A (BoNT/A) and U0126 in hypersensitivity after STZ induction. (A, B, C) BoNT/A, a neurotoxic protein produced by the bacterium *Clostridium botulinum*, and (D, E, F) U0126, a potent and selective MAPKs kinase 1/2 inhibitor, were used to STZ-induced diabetic rats by an intraplantar (i.pl.) injection for evaluating its effects on (A, D) thermal hyperalgesia, (B, E) mechanical hyperalgesia and (C, F) mechanical allodynia. The withdrawal latency, withdrawal threshold, and mechanical threshold were represented as the mean ± SD. The properties of BoNT/A were tested at the concentration of vehicle (white circles), 3U/kg (light blue circles), 5U/kg (blue circles), and 7U/kg (deep blue circles) (n = 4 per group). The properties of U0126 were verified at the concentration of vehicle (white circles), 1 μM (light pink circles), 20 μM (deep pink circles), and 50 μM (red circles) (n = 4 per group). Negative control was demonstrated by an i.pl. U0124 50 μM injection (purple circles), an inactive analog of U0126, in STZ-induced diabetic rats (n = 4). Statistical comparisons were made by a two-way ANOVA, followed by Bonferroni *post hoc* test, with the concentrations of BoNT/A or U0126 as between-subjects factors and time as the within-subjects factor (For interpretation of the references to colour in this figure legend, the reader is referred to the web version of this article).

to PIH 6. Conversely, withdrawal latencies at PIH 24 were indicated as a condition of thermal hyperalgesia. In the Vehicle group, STZ-induced diabetic rats displayed similar withdrawal latencies from PIH 1 to PIH 24 (*vs.* PIH 0, $p > 0.05$, respectively).

U0126 significantly affected an increase of withdrawal thresholds ($F = 1.69$; $p = 0.0451$) dose dependently ($F = 32.70$; $p < 0.0001$) and changed the temporal pattern of mechanical hyperalgesia ($F = 4.34$; $p = 0.0003$) after STZ induction (Fig. 6E). In the U0126 50 μM group, withdrawal thresholds increased rapidly and continued from PIH 1 to PIH 6; however, withdrawal thresholds at PIH 24 gradually reverted to mechanical hyperalgesia. Following STZ induction, the effects of U0126 on mechanical thresholds did not expose any significant difference ($F = 1.45$; $p = 0.1168$) in a dose-responsive manner ($F = 0.87$; $p = 0.4587$) and did not alter the time-based pattern of mechanical allodynia ($F = 0.48$; $p = 0.8500$) (Fig. 6F). For example, STZ-induced mechanical thresholds in the U0126 50 μM group showed equivalent values from PIH 1 to PIH 6 and at PIH 24. Additionally, U0124 50 μM did not influence withdrawal latency, withdrawal thresholds, and mechanical thresholds form PIH 1 to PIH 6 and at PIH 24 ($p > 0.05$, respectively).

3.9. Effects of U0126 on STZ-induced SP-, CGRP- and pERK1/2-IR in SENFs

To elucidate the effects of U0126 on STZ-induced morphological changes in the skin, the distribution of SP-, CGRP-, and pERK1/2-IR SENFs were assessed at PIH 6 following i.pl. injection (Fig. 7). SP-IR SENFs in the Vehicle group originated from dermal nerve fascicles and showed beaded shapes in the subepidermal nerve plexus (Fig. 7A). In the U0126 50 μM group, U0126 resulted in a dramatic loss of SP-IR SENFs (Fig. 7B). There was a significant difference in areas of SP-IR SENFs between the Vehicle group and the U0126 50 μM group ($p = 0.0002$) (Fig. 7C). In the Vehicle group, the irregular shapes of CGRP-IR SENFs close to the epidermal–dermal junction withdrew to dermal nerve fascicles (Fig. 7D). The partial reduction of CGRP-IR SENFs in the U0126 50 μM group was clearly shown in dermal nerve fascicles (Fig. 7E). The quantitative areas of CGRP-IR SENFs exposed a significant difference between the Vehicle group and the U0126 50 μM group ($p = 0.0142$) (Fig. 7F). pERK1/2-IR SENFs in the Vehicle group displayed linear shapes in dermal nerve fascicles with tiny sprouting nerve terminals around the epidermal–dermal junction (Fig. 7G). In the U0126 50 μM group, only few fragmented pERK1/2-IR SENFs were observed (Fig. 7H). Areas of pERK1/2-IR SENFs in the Vehicle group were significantly different than those in the U0126 50 μM group ($p < 0.0001$).

3.10. Role of BoNT/A in SP-, CGRP- and pERK1/2-IR SENFs following STZ induction

To illustrate the role of BoNT/A in STZ-induced morphological changes in the skin, the distributions of SP-, CGRP-, and pERK1/2-IR SENFs were evaluated at PID 3 and PID 14 after i.pl. injection (Fig. 8). After i.pl. BoNT/A 7U/kg injection, a few fragmented SP-IR SENFs were detected in the subepidermal nerve plexus at PID 3 (Fig. 8A). SP-IR that slightly increased in SENFs showed beaded shapes at PID 14 (Fig. 8B). The quantitative values in the BoNT/A 7U/kg group compared with those in the Vehicle group indicated that BoNT/A 7U/kg significantly diminished areas of SP-IR SENFs ($p < 0.0001$ at PID 3 and $p = 0.0010$

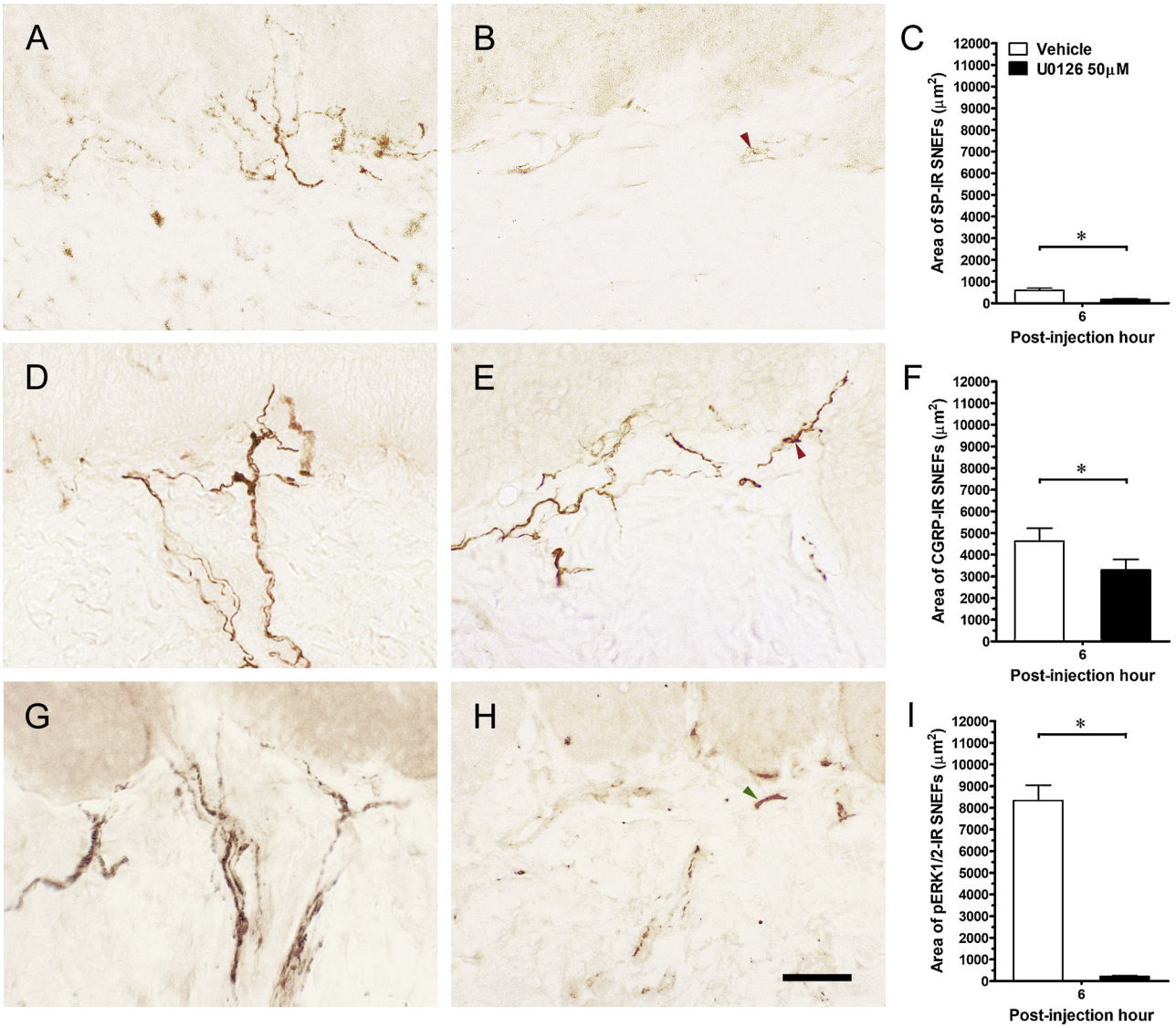

Fig. 7. Influence of U0126 on STZ-induced SENFs distribution. The sections were immunostained with the antisera against (A, B) SP, (D, E) CGRP and (G, H) pERK1/2. Graphs showed the efficacy of U0126 at post injection hour (PIH) 6 in.(A, D, G) the Vehicle group and (B, E, H) the U0126 50 μM group after STZ induction. (C, F, I) Panels revealed the quantitative IR SENFs areas. In the U0126 50 μM group, peptidergic SENFs presented the few varicosities or swelling appearances (red arrowhead) in the subepidermal plexus adjacent to epidermal-dermal junction, where pERK1/2-IR SENFs exhibited the short fragments (green arrowhead). The alterations of SENFs distribution in the Vehicle group (open bars) and the U0126 50 μM group (fill bars) were quantified at PIH 6 by the results of IR, which were represented as the area of IR SENFs (mean ± SD; n = 4 per group). Student's *t* test was applied to examine the differences against the results of the Vehicle group. Scale bar = 50 μm (For interpretation of the references to colour in this figure legend, the reader is referred to the web version of this article).

at PID 14) (Fig. 8C). Notably, PID 3 and PID 14 differed significantly in the BoNT/A 7U/kg group ($p = 0.0017$). In the BoNT/A 7U/kg group, limited CGRP-IR in SENFs were identified at PID 3 in dermal nerve fascicles, with enlarged swelling of the nerve terminal adjacent to the epidermal–dermal junction (Fig. 8D). Numerous CGRP-IR SENFs increased in dermal nerve fascicles and clearly formed the subdermal nerve plexus at PID 14 (Fig. 8E). The quantitative values in the BoNT/A 7U/kg group suggested that BoNT/A 7U/kg had an intense effect on decreased areas of CGRP-IR SENFs, which were comparable with the Vehicle group ($p < 0.0001$ at PID 3 and $p = 0.0108$ at PID 14) (Fig. 8F). In the BoNT/A 7U/kg group, the values of areas of CGRP-IR SENFs significantly intensified at PID 14 ($p = 0.0004$). Several pERK1/2-IR SENFs in the BoNT/A 7U/kg group presented as irregular lines close to the epidermal–dermal junction at PID 3 (Fig. 8G). pERK1/2-IR largely increased in SENFs at PID 14, showing in dermal nerve fascicles and visibly forming the subdermal nerve plexus (Fig. 8H). The quantitative values compared with the Vehicle group confirmed that BoNT/A 7U/kg significantly reduced areas of pERK1/2-IR SENFs ($p < 0.0001$ at PID 3 and $p = 0.0002$ at PID 14) (Fig. 8I). Between PID 3 and PID 14, there was a significant difference in the BoNT/A 7U/kg group ($p = 0.0001$).

3.11. Influence of TRPV channel antagonists on STZ-induced hypersensitivity and distribution of SENFs

It was hypothesized that phosphorylation of ERK1/2 in SENFs might influence TRPV channel release of neuropeptides that induce hypersensitivity. Therefore, TRPV1 channel antagonist, capsazepine, and TRPV4 channel antagonist, RN-1734, were selected to block TRPV channels by i.pl. injection. Additionally, changes of values were evaluated for areas of SP-, CGRP-, and pERK1/2-IR SENFs (Fig. 9). With STZ induction, the local effects of TRPV channel antagonists produced a dose-dependent (capsazepine: $F = 108.3$, $p < 0.0001$; RN-1734: $F = 58.61$, $p < 0.0001$) significant increase of withdrawal latency

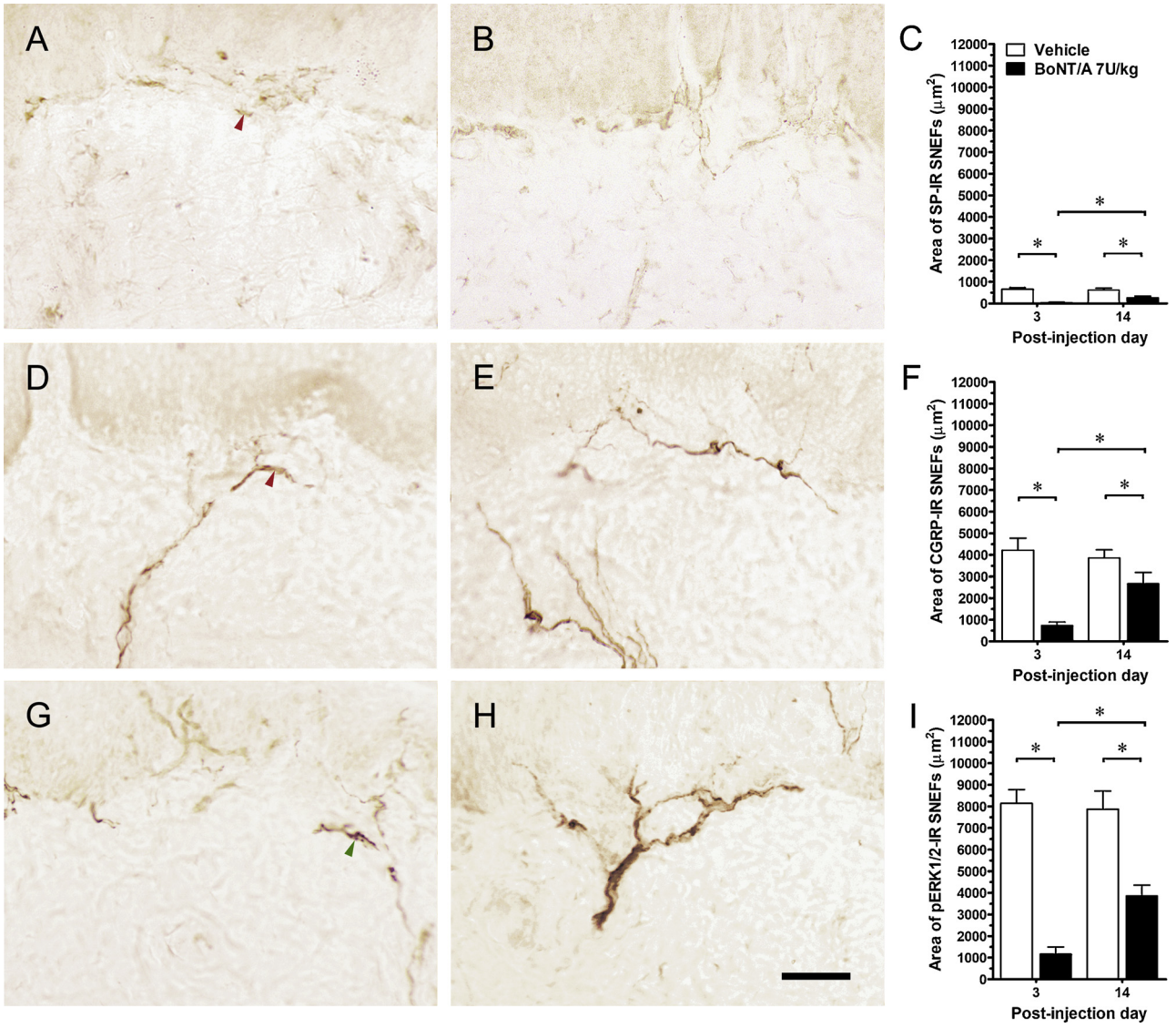

Fig. 8. Effects of Botulinum toxin type A (BoNT/A) on SENFs distribution after STZ induction. The sections were immunostained with the antisera against (A, B) SP, (D, E) CGRP and (G, H) pERK1/2. Graphs showed the effectiveness of BoNT/A in the BoNT/A 7U/kg group at (A, D, G) post injection day (PID) 3 and (B, E, H) PID 14 after STZ induction. (C, F, I) Panels revealed the quantitative IR SENFs areas. In the BoNT/A 7U/kg group, peptidergic SENFs at PID 3 presented rare beaded varicosities or swelling forms (red arrowhead) in the subepidermal plexus nearby epidermal-dermal junction, where pERK1/2-IR SENFs exhibited the irregular fragments (green arrowhead). The time-dependent changes of SENFs distribution in the Vehicle group (open bars) and the BoNT/A 7U/kg group (fill bars) were quantified at PID 3 and PID 14 by the results of IR, which were represented as the area of IR SENFs (mean ± SD; n = 4 per group). Student's *t* test was applied to examine the differences against the values of the Vehicle group at two time point. Scale bar = 50 μm (For interpretation of the references to colour in this figure legend, the reader is referred to the web version of this article).

(capsazepine: F = 6.84, $p < 0.0001$; RN-1734: F = 3.40, $p < 0.0001$) and changed the temporal pattern of thermal hyperalgesia (capsazepine:F = 31.96, $p < 0.0001$; RN-1734: F = 17.42, $p < 0.0001$) (Fig. 9A and D). TRPV channel antagonists significantly increased STZ-induced withdrawal thresholds (capsazepine: F = 1.88, $p = 0.0207$; RN-1734: F = 1.28, $p = 0.2083$) in a dose-responsive manner (capsazepine: F = 29.33, $p < 0.0001$; RN-1734: F = 23.28, $p < 0.0001$) and altered the time-based pattern of mechanical hyperalgesia (capsazepine: F = 17.42, $p < 0.0001$; RN-1734: F = 10.34, $p < 0.0001$) (Fig. 9B and E). After STZ induction, the effects of TRPV channel antagonists on mechanical thresholds (capsazepine: F = 4.345, $p < 0.0001$; RN-1734: F = 2.92, $p = 0.0002$) exhibited a significant dose-dependent increase (capsazepine: F = 69.17, $p < 0.0001$; RN-1734: F = 53.84, $p < 0.0001$) and changed the time-based pattern of mechanical allodynia (capsazepine: F = 22.84, $p < 0.0001$; RN-1734: F = 17.57, $p < 0.0001$) (Fig. 9C and F).

In the capsazepine 25 mM group, capsazepine resulted in a decrease of areas of SP-IR SENFs that were more significant than those in the Vehicle group ($p = 0.0005$) (Fig. 9G). Quantitative areas of CGRP-IR SENFs revealed a significant difference between the capsazepine 25 mM group and the Vehicle group ($p = 0.0089$). Areas of pERK1/2-IR SENFs in the capsazepine 25mM group were significantly different than those in the Vehicle group ($p < 0.0001$). The quantitative values compared with the Vehicle group indicated that RN-1734 120mM reduced areas of SP-IR SENFs significantly ($p = 0.0003$) (Fig. 9H). The quantitative values suggested that RN-1734 120 mM had an intense effect on the decreased areas of CGRP-IR SENFs, which paralleled the Vehicle group ($p = 0.0007$). Quantitative areas of pERK1/2-IR SENFs confirmed that RN-1734 120mM had a noticeable effect on pERK1/2-IR, which significantly paralleled the Vehicle group ($p < 0.0001$).

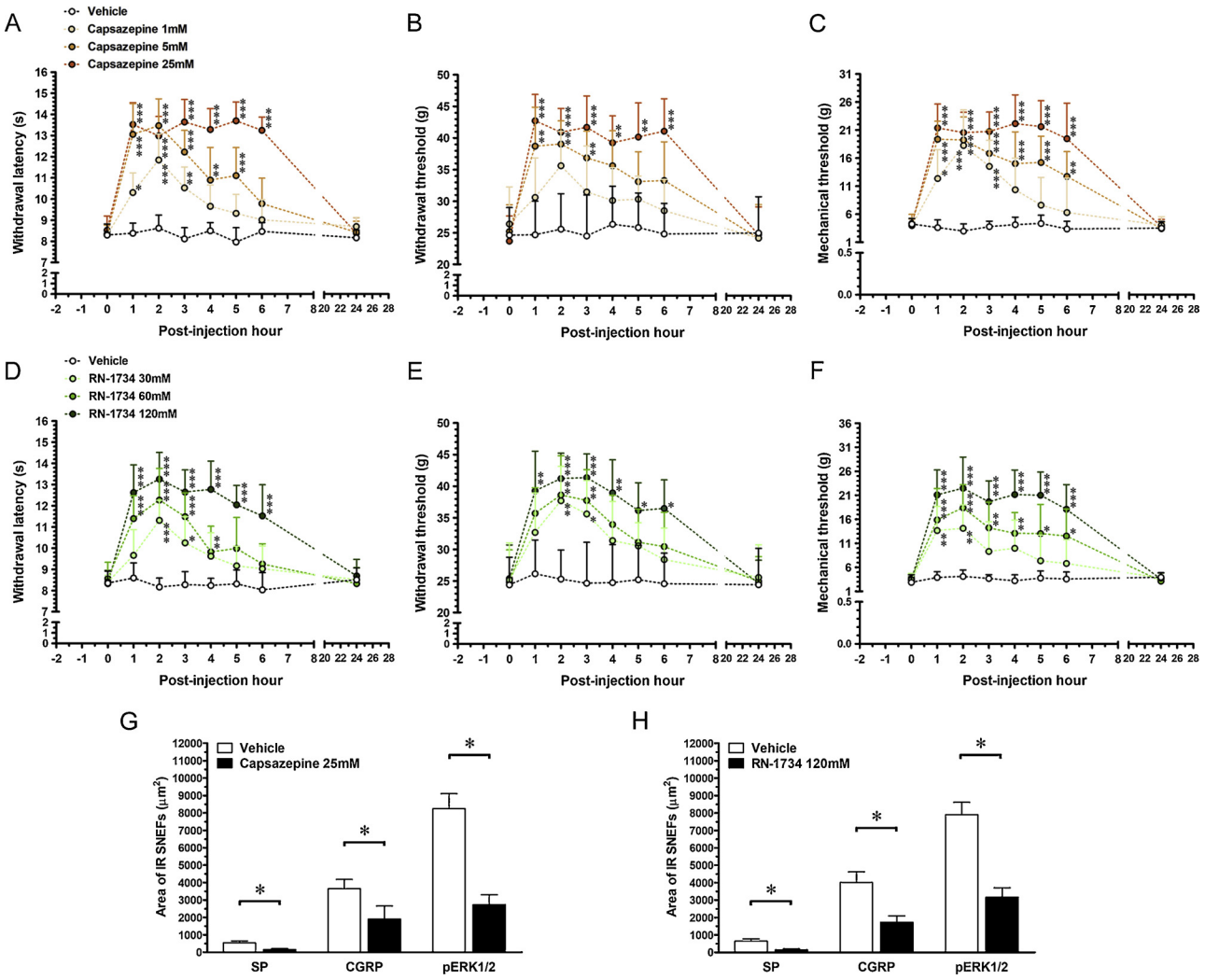

Fig. 9. Role of transient receptor potential vanilloid (TRPV) channel antagonists in STZ-induced hypersensitivity and SENFs distribution. (A, B, C) TRPV1 channel antagonist, capsazepine, and (D, E, F) TRPV4 channel antagonist, RN-1734, were selected to block TRPV channels in STZ-induced diabetic rats by an i.pl. injection for evaluating its effects on (A, D) thermal hyperalgesia, (B, E) mechanical hyperalgesia and (C, F) mechanical allodynia. The withdrawal latency, withdrawal threshold, and mechanical threshold were represented as the mean ± SD. The properties of capsazepine were tested at the concentration of vehicle (white circles), 1 mM (light orange circles), 5 mM (orange circles), and 25 mM (deep orange circles) (n = 4 per group). The properties of RN-1734 were verified at the concentration of vehicle (white circles), 30 μM (light green circles), 60 μM (green circles), and 120 μM (deep green circles) (n = 4 per group). Statistical comparisons were made by a two-way ANOVA, followed by Bonferroni *post hoc* test, with the concentrations of TRPV channel antagonists as between-subjects factors and time as the within-subjects factor. (G, H) The changes of SENFs distribution in the Vehicle group (open bars) and the Capsazepine 25 mM group or the RN-1734 120 mM group (fill bars) were quantified at PIH 6 by the results of IR, which were represented as the area of IR SENFs (mean ± SD; n = 4 per group). Student's *t* test was applied to examine the differences against the results of the Vehicle group (For interpretation of the references to colour in this figure legend, the reader is referred to the web version of this article).

4. Discussions

Cumulative evidence suggest that hyperglycemia and hypersensitivity are not correlated in rats following STZ induction (Grote and Wright, 2016; Bishnoi et al., 2011; Cunha et al., 2009; Romanovsky et al., 2006). According to our laboratory data, STZ-induced diabetic rats with blood glucose levels less than 400 mg/dl still exhibited thermal hyperalgesia, mechanical hyperalgesia and mechanical allodynia. Thus, it is reasonable to propose that STZ-induced hyperglycemia was a result of insulin deficiency, known as insulinopenia in the clinical diagnosis. In view of that, Guo et al. report that an i.pl. insulin injection attenuates mechanical hyperalgesia in STZ-induced diabetic C57BL/6 J mice (Guo et al., 2011). Moreover, treating STZ-induced diabetic rats with insulin reveals an improvement in gastrointestinal symptoms (Lin et al., 2008). Interestingly, local hyperglycemia in both the sciatic nerve and the DRG by perfusion with a high-glucose solution also causes obvious mechanical hyperalgesia in rats (Dobretsov et al., 2003 and 2001). Taken together, these data indicate that chronic effects of hyperglycemia results in a phenomenon referred to as the glucose neurotoxicity.

Skin biopsy combined with quantitative density of PGP9.5-IR IENFs has become an established pathological approach for the clinical diagnosis of human type 1 and type 2 DM (Polydefkis et al., 2001; Sumner et al., 2003; Shun et al., 2004). It is known that density of PGP9.5-IR IENFs is significantly decreased in both human type 1 and type 2 DM (Cheng et al., 2013; Shun et al., 2004). In STZ-induced diabetic rats, PGP9.5-IR IENFs and epidermal thickness are affected in the glabrous skin (Boric et al., 2013; Calcutt, 2004). These PGP9.5-IR IENFs are degenerated and even fail to penetrate epidermis, and often forming fragmented subepidermal nerve plexus and nerve fascicles in dermis (Kennedy et al., 1996). In consistent with the previous studies, we found that PGP9.5-IR reduced in SENFs during the entire experimental

period after STZ induction. Furthermore, peripherin-IR SENFs exhibited obvious nerve terminal swellings and declined in dermal nerve fascicles, indicating the degeneration of unmyelinated C and myelinated A-delta nerve fibers. Additionally, we found a decrease of NF200-IR SENFs, presenting as the degeneration of myelinated A-beta nerve fibers. Similar results have also been observed in STZ-induced diabetic mice skin (Yasuda et al., 2003). These data suggest that partial nerve degeneration occurs in all the phenotypes of SENFs, which may be a reason for developing hypersensitivity after STZ induction.

In patients with type 1 DM, immunohistochemistry reveals four neuropeptides, including SP, CGRP, vasoactive intestinal polypeptide, and neuropeptide Y, are decreased in IENFs (Pinho-Ribeiro et al., 2017). These neuropeptides expressed in unmyelinated C fibers are either SP and/or CGRP, and myelinated A-delta fibers are entirely expressed as CGRP (Ko et al., 2014; Johnson et al., 2008). It has been reported that early treatment with insulin prevents STZ-induced nerve denervation in gastric mucosa, where SP- or CGRP-IR nerve fibers are preserved (Lin et al., 2008). In the existing results, an obvious decrease of SP-IR SENFs was detected in subepidermal nerve plexus, and reduced CGRP-IR SENFs were mostly observed in dermal nerve fascicles following STZ induction. Based on these results, the integrity of peptidergic SENFs was altered in STZ-induced diabetic rat skin, which provides opportunities to examine the correlation between neuropeptides and hypersensitivity.

An enhanced release of neuropeptides from primary afferents promotes the degranulation of mast cells and recruitment of circulating neutrophils, macrophages and T cells, known as the neurogenic inflammation (Pinho-Ribeiro et al., 2017; Choi and Di Nardo, 2018). Nerve growth factor (NGF) is considered as a major neurotrophin, which is released from these immune cells and involved in neuroimmune interactions (Khodorova et al., 2013; Osikowicz et al., 2013; Ji et al., 2002). Neurotrophin binding to tyrosine kinase A (TrkA) receptor and p75 pan-neurotrophin receptor (NTR) activates signaling cascades, which further regulating the release of neuropeptides (Pezet et al., 2002; Khodorova et al., 2013; Fernyhough et al.,1995). Moreover, it has been proposed that endocytosis of NGF can regulate axonal retrograde transport from the skin to the DRG to modulate the synthesis of neuropeptides (Lindsay and Harmar, 1989; Goedert et al., 1981). Therefore, the decrease of peptidergic SENFs in STZ-induced diabetic rat skin may be resulted from the elevation of SP and CGRP releasing which regulated by activation of neurotrophin cascades.

Recently, a subcutaneous BoNT/A injection administrated in patients with type 1 DM blocks the release of neuropeptides, with successful relief of hypersensitivity (Ghasemi et al., 2014; Yuan et al., 2009; Kumar, 2018; Paterson et al., 2014). Furthermore, the acceptance of BoNT/A for the treatment of hypersensitivity has also been illustrated its analgesic properties in the rodent models of inflammatory and neuropathic pain (Lee et al., 2011; Favre-Guilmard et al., 2009; Bach-Rojecky et al., 2005). In the present study, we confirmed that STZ-induced thermal hyperalgesia, mechanical hyperalgesia, and mechanical allodynia were attenuated by an i.pl. BoNT/A injection dose-dependently. The analgesic effects of BoNT/A are by the reduced release of neuropeptides from primary afferents, revealing a direct peripheral inhibition of hypersensitivity (Park and Park, 2017; Guo et al., 2013). The long lasting analgesic effects of BoNT/A may be induced by axonal retrograde transport to the DRG and even by axonal anterograde transport to the spinal cord, resulting in an indirect central inhibition of hypersensitivity (Park and Park, 2017). Although BoNT/A can block the release of neuropeptides, we found a further decrease of SP- and CGRP-IR SENFs in STZ-induced diabetic rat skin. This efficacy of BoNT/A on the reduction of CGRP-IR IENFs and CGRP contents in the skin is also been observed in a mice model of TRPV1 channel-depleted neuropathy (Hsieh et al., 2012). We suppose that blockage of release of neuropeptides may favor the degradation of neuropeptides in synaptic vesicles by cytosolic proteases, providing an explanation for the decrease of these detectable peptidergic SENFs in STZ-induced diabetic rat skin. Due to the increase of SP- and CGRP-IR SENFs at PID14 following i.pl. BoNT/A injection, we suggested the newly synthesized neuropeptides allow comparatively restoration in synaptic vesicles.

The multiple receptors, including ionotropic glutamate receptor (GluR), metabotropic GluR, neurokinin-1 receptor, and TrkA receptor, are involved in the modulation of ERK1/2 (Sandkühler, 2007; Kawasaki et al., 2004; Pezet et al., 2002). In STZ-induced diabetic rats, the binding of NGF to TrkA receptor and/or p75 NTR causes the activation of signaling cascades in the nerve and the DRG, where ERK1/2 and p38 kinases are phosphorylated (Khodorova et al., 2013; Ji et al., 2002; Fernyhough et al., 1995). Our study further revealed that these observations were extended to the STZ-induced diabetic rat skin, where increased pERK1/2-IR SENFs were consistently sustained until the second month after STZ induction. Double immunofluorescence showed that a portion of pERK1/2-IR SENFs was colocalized with SP- or CGRP-IR SENFs. It implies that activation of ERK1/2 in primary afferents may be closely linked to the release of neuropeptides that induces hypersensitivity.

U0126 attenuates capsaicin- and NGF-evoked thermal hyperalgesia, which is like the property of phosphatidylinositol 3-kinase inhibitor through an i.pl. injection (Zhuang et al., 2004). In the present study, we concluded that an i.pl. U0126 injection attenuated STZ-induced thermal hyperalgesia and mechanical hyperalgesia in a dose-responsive manner, but had no effect on mechanical allodynia. Based on our morphologic evidence, an i.pl. U0126 50 μM injection diminished pERK1/2- and SP-IR SENFs rapidly, whereas a portion of CGRP-IR SENFs was reserved. Moreover, the comparable decreased pattern of pERK1/2-IR SENFs was also exposed following an i.pl. BoNT/A 7U/kg injection. These results suggested that neurogenic inflammation might be further associated with the phosphorylation of ERK1/2 in primary afferents. Together, we reveal a correlation between pERK1/2-IR SENFs and hyperalgesia, and propose a therapeutic potential of ERK inhibitor in the human type 1 DM.

Neuropeptides are generally storage in synaptic vesicles, large dense-core vesicles, and released through an ion channel-dependent calcium influx and SNARE protein-mediated membrane fusion (Zhao et al., 2011; Gustavsson et al., 2012). Synaptic vesicles are also served as carriers of ion channels, including TRPV1, TRPV4, and TRP ankyrin 1 (TRPA1) channels (Srebro et al., 2016; Cui et al., 2014; Zhao et al., 2011). TRP channels in primary afferents are critical in the regulation of exocytosis of synaptic vesicles and recruitment of the new TRP channels (Devesa et al., 2014; Meng et al., 2016; Lamarre and Bjorling, 2015). Thus, we suggest that TRP channels modulate the release of neuropeptides, which is linked to the increased translocation of the new TRPV channels to the plasma membrane for developing STZ-induced hypersensitivity. Capsazepine, the TRPV1 channel antagonist, indicates the capsaicin-evoked hypersensitivity, but not the cutaneous vasodilation and edema, was improved (Gouin et al., 2017). Our present data revealed the therapeutic effects of capsazepine on STZ-induced thermal hyperalgesia, mechanical hyperalgesia, and mechanical allodynia were dose dependently. Remarkably, Kistner et al. reveal that capsazepine also acts as the TRPA1 channel agonist that causes sustained TRPA1 desensitization to inhibit neurogenic inflammation in mice model of dextran sulphate sodium colitis, even providing its intense effects on thermal hypoalgesia in naïve mice (Kistner et al., 2016). Additionally, our present study illustrated that the TRPV4 specific antagonist, RN-1734, are like capsazepine for the reduction of thermal hyperalgesia, mechanical hyperalgesia, and mechanical allodynia. These results are in agreed with a recent study showing that magnesium sulfate solution-induced mechanical hyperalgesia is attenuated by RN-1734 (Srebro et al., 2016). It supports an idea that TRPV4 channel antagonists could be another choice as an analgesic drug in the treatment of hypersensitivity in human type 1 DM.

Several signaling cascades, containing the protein kinase A (PKA), PKB (Akt), PKC, ERK1/2, and calcium/calmodulin-dependent protein kinase II, have been involved in sensitizing TRPV1 channel (Luo et al.,

2015; Zhuang et al., 2004; Clapham, 2003). Furthermore, it has been shown that TRPV1 channel is colocalized with phosphorylated ERK1/2 in most small-diameter DRG neurons, which mediates capsaicin- and NGF-evoked thermal hyperalgesia (Zhuang et al., 2004). An i.pl. capsazepine 25 mM injection reduced peptidergic- and pERK1/2-IR SENFs. Comparable results also show the effective local and systemic treatments with capsazepine decrease the released CGRP contents measured in the colon and the skin (Kistner et al., 2016). It is also linked to a previously report that increased TRPV1 channel contributes to STZ-induced thermal hyperalgesia in mice (Pabbidi et al., 2008). Furthermore, our morphological evidence confirmed that RN-1734 was also efficiently reduced peptidergic- and pERK1/2-IR SENFs after STZ induction. Collectively, these results suggest that translocation of the new TRP channels may be modulated by ERK1/2 activation in primary afferents for the development of hypersensitivity.

In conclusion, the present study demonstrated that (1) PGP9.5-, peripherin-, and NF200-IR SENFs were reduced; (2) there were large decreases of SP- and CGRP-IR SENFs; (3) pERK1/2- and ERK-IR were significantly increased in SENFs; (4) an i.pl. BoNT/A injection attenuated thermal hyperalgesia, mechanical hyperalgesia, and mechanical allodynia; (5) pERK-IR SENFs mediated thermal hyperalgesia and mechanical hyperalgesia, which were proven by an i.pl. U0126 injection; (6) TRPV channel antagonists, capsazepine and RN-1734, reduce thermal hyperalgesia, mechanical hyperalgesia, and mechanical allodynia by an i.pl. injection; and (7) By studying the local analgesic effects, peptidergic- and pERK1/2-IR SENFs were efficiently decreased. Taken together, our observations suggest the phosphorylation of ERK1/2 in SENFs may participate in sensitizing TRPV channels, which mediate the release of neuropeptides and the translocation of the new TRPV channels for developing STZ-induced hyperalgesia, providing novel therapeutic strategies for targeting medications in the skin.

Funding

This work was supported by the National Science Council (102-2320-B-040-024-), Ministry of Science and Technology (104-2320-B-040-012-, 107-2320-B-040-024-) and Chung Shan Medical University (G102N0003, F106N0009), Taiwan.

Declaration of conflicting interests

The authors declare that they have no competing interests.

References

Aley, K.O., Martin, A., McMahon, T., Mok, J., Levine, J.D., Messing, R.O., 2001. Nociceptor sensitization by extracellular signal-regulated kinases. J. Neurosci. 21 (17), 6933–6939.

Bach-Rojecky, L., Relja, M., Lackovic, Z., 2005. Botulinum toxin type A in experimental neuropathic pain. J. Neural. Trans. 112 (2), 215–219.

Bishnoi, M., Bosgraaf, C.A., Abooj, M., Zhong, L., Premkumar, L.S., 2011. Streptozotocin-induced early thermal hyperalgesia is independent of glycemic state of rats: role of transient receptor potential vanilloid 1(TRPV1) and inflammatory mediators. Mol. Pain 7, 52.

Boric, M., Skopljanac, I., Ferhatovic, L., Jelicic Kadic, A., Banozic, A., Puljak, L., 2013. Reduced epidermal thickness, nerve degeneration and increased pain-related behavior in rats with diabetes type 1 and 2. J. Chem. Neuroanat. 53, 33–40.

Calcutt, N.A., 2004. Experimental models of painful diabetic neuropathy. J. Neurol. Sci. 220 (1–2), 137–139.

Callaghan, B.C., Cheng, H.T., Stables, C.L., Smith, A.L., Feldman, E.L., 2012. Diabetic neuropathy: clinical manifestations and current treatments. Lancet Neurol. 11 (6), 521–534.

Cheng, H.T., Dauch, J.R., Porzio, M.T., Yanik, B.M., Hsieh, W., Smith, A.G., Singleton, J.R., Feldman, E.L., 2013. Increased axonal regeneration and swellings in intraepidermal nerve fibers characterize painful phenotypes of diabetic neuropathy. J. Pain 14 (9), 941–947.

Chien, H.F., Tseng, T.J., Lin, W.M., Yang, C.C., Chang, Y.C., Chen, R.C., Hsieh, S.T., 2001. Quantitative pathology of cutaneous nerve terminal degeneration in the human skin. Acta Neuropathol. 102 (5), 455–461.

Choi, J.E., Di Nardo, A., 2018. Skin neurogenic inflammation. Semin. Immunopathol. 40 (3), 249–259.

Clapham, D.E., 2003. TRP channels as cellular sensors. Nature 426 (6966), 517–524.

Committee, I.A.S.P., 1980. Ethical standards for investigations of experimental pain in animals. The Committee for Research and Ethical Issues of the International Association for the Study of Pain. Pain 9 (2), 141–143.

Cui, Y.Y., Xu, H., Wu, H.H., Qi, J., Shi, J., Li, Y.Q., 2014. Spatio-temporal expression and functional involvement of transient receptor potential vanilloid 1 in diabetic mechanical allodynia in rats. PLoS One 9 (7), e102052.

Cunha, J.M., Funez, M.I., Cunha, F.Q., Parada, C.A., Ferreira, S.H., 2009. Streptozotocin-induced mechanical hypernociception is not dependent on hyperglycemia. Braz. J. Med. Biol. Res. 42 (2), 197–206.

Devesa, I., Ferrándiz-Huertas, C., Mathivanan, S., Wolf, C., Luján, R., Changeux, J.P.3, Ferrer-Montiel, A., 2014. αCGRP is essential for algesic exocytotic mobilization of TRPV1 channels in peptidergic nociceptors. Proc. Natl. Acad. Sci. 111 (51), 18345–18350.

Dobretsov, M., Hastings, S.L., Stimers, J.R., Zhang, J.M., 2001. Mechanical hyperalgesia in rats with chronic perfusion of lumbar dorsal root ganglion with hyperglycemic solution. J. Neurosci. Methods 110 (1–2), 9–15.

Dobretsov, M., Hastings, S.L., Romanovsky, D., Stimers, J.R., Zhang, J.M., 2003. Mechanical hyperalgesia in rat models of systemic and local hyperglycemia. Brain Res. 960 (1–2), 174–183.

Favre-Guilmard, C., Auguet, M., Chabrier, P.E., 2009. Different antinociceptive effects of botulinum toxin type A in inflammatory and peripheral polyneuropathic rat models. Eur. J. Pharmacol. 617 (1–3), 48–53.

Fernyhough, P., Diemel, L.T., Hardy, J., Brewster, W.J., Mohiuddin, L., Tomlinson, D.R., 1995. Human recombinant nerve growth factor replaces deficient neurotrophic support in the diabetic rat. Eur. J. Neurosci. 7 (5), 1107–1110.

Ghasemi, M., Ansari, M., Basiri, K., Shaigannejad, V., 2014. The effects of intradermal botulinum toxin type A injections on pain symptoms of patients with diabetic neuropathy. J. Res. Med. Sci. 19 (2), 106–111.

Giannini, C., Dyck, P.J., 1994. Ultrastructural morphometric abnormalities of sural nerve endoneurial microvessels in diabetes mellitus. Ann. Neurol. 36 (3), 408–415.

Goedert, M., Stoeckel, K., Otten, U., 1981. Biological importance of the retrograde axonal transport of nerve growth factor in sensory neurons. Proc. Natl. Acad. Sci. 78, 5895–5898.

Gouin, O., L'Herondelle, K., Lebonvallet, N., Le Gall-Ianotto, C., Sakka, M., Buhé, V., Plée-Gautier, E., Carré, J.L., Lefeuvre, L., Misery, L., Le Garrec, R., 2017. TRPV1 and TRPA1 in cutaneous neurogenic and chronic inflammation: pro-inflammatory response induced by their activation and their sensitization. Protein Cell 8 (9), 644–661.

Grote, C.W., Wright, D.E., 2016. A role for insulin in diabetic neuropathy. Front. Neurosci. 10, 581.

Guo, G., Kan, M., Martinez, J.A., Zochodne, D.W., 2011. Local insulin and the rapid regrowth of diabetic epidermal axons. Neurobiol. Dis. 43 (2), 414–421.

Guo, B.L., Zheng, C.X., Sui, B.D., Li, Y.Q., Wang, Y.Y., Yang, Y.L., 2013. A closer look to botulinum neurotoxin type A-induced analgesia. Toxicon 71, 134–139.

Gustavsson, N., Wu, B., Han, W., 2012. Calcium sensing in exocytosis. Adv. Exp. Med. Biol. 740, 731–757.

Hirai, A., Yasuda, H., Joko, M., Maeda, T., Kikkawa, R., 2000. Evaluation of diabetic neuropathy through the quantitation of cutaneous nerves. J. Neurol. Sci. 172 (1), 55–62.

Hsieh, Y.L., Lin, C.L., Chiang, H., Fu, Y.S., Lue, J.H., Hsieh, S.T., 2012. Role of peptidergic nerve terminals in the skin: reversal of thermal sensation by calcitonin gene-related peptide in TRPV1-depleted neuropathy. PLoS One 7 (11), e50805.

Ji, R.R., Baba, H., Brenner, G.J., Woolf, C.J., 1999. Nociceptive-specific activation of ERK in spinal neurons contributes to pain hypersensitivity. Nat. Neurosci. 2 (12), 1114–1119.

Ji, R.R., Samad, T.A., Jin, S.X., Schmoll, R., Woolf, C.J., 2002. p38 MAPK activation by NGF in primary sensory neurons after inflammation increases TRPV1 levels and maintains heat hyperalgesia. Neuron 36 (1), 57–68.

Johnson, G.L., Lapadat, R., 2002. Mitogen-activated protein kinase pathways mediated by ERK, JNK, and p38 protein kinases. Science 298 (5600), 1911–1912.

Johnson, M.S., Ryals, J.M., Wright, D.E., 2008. Early loss of peptidergic intraepidermal nerve fibers in an STZ-induced mouse model of insensate diabetic neuropathy. Pain 140 (1), 35–47.

Kawasaki, Y., Kohno, T., Zhuang, Z.Y., Brenner, G.J., Wang, H., Van Der, M.C., Befort, K., Woolf, C.J., Ji, R.R., 2004. Ionotropic and metabotropic receptors, protein kinase A, protein kinase C, and Src contribute to C-fiber-induced ERK activation and cAMP response element-binding protein phosphorylation in dorsal horn neurons, leading to central sensitization. J. Neurosci. 24 (38), 8310–8321.

Kennedy, W.R., Wendelschafer-Crabb, G., Johnson, T., 1996. Quantitation of epidermal nerves in diabetic neuropathy. Neurology 47 (4), 1042–1048.

Khodorova, A., Nicol, G.D., Strichartz, G., 2013. The p75NTR signaling cascade mediates mechanical hyperalgesia induced by nerve growth factor injected into the rat hind paw. Neuroscience 254, 312–323.

Kistner, K., Siklosi, N., Babes, A., Khalil, M., Selescu, T., Zimmermann, K., Wirtz, S., Becker, C., Neurath, M.F., Reeh, P.W., Engel, M.A., 2016. Systemic desensitization through TRPA1 channels by capsazepine and mustard oil - a novel strategy against inflammation and pain. Sci. Rep. 6, 28621.

Ko, M.H., Hu, M.E., Hsieh, Y.L., Lan, C.T., Tseng, T.J., 2014. Peptidergic intraepidermal nerve fibers in the skin contribute to the neuropathic pain in paclitaxel-induced peripheral neuropathy. Neuropeptides 48 (3), 109–117.

Ko, M.H., Hsieh, Y.L., Hsieh, S.T., Tseng, T.J., 2015. Nerve demyelination increases metabotropic glutamate receptor subtype 5 expression in peripheral painful mononeuropathy. Int. J. Mol. Sci. 16 (3), 4642–4665.

Ko, M.H., Yang, M.L., Youn, S.C., Lan, C.T., Tseng, T.J., 2016. Intact subepidermal nerve fibers mediate mechanical hypersensitivity via the activation of protein kinase C gamma in spared nerve injury. Mol. Pain 12, 1–15.

Kumar, R., 2018. Therapeutic use of botulinum toxin in pain treatment. Neuronal Signal. 2 (3) NS20180058.
Lamarre, N.S., Bjorling, D.E., 2015. Treatment of painful bladder syndrome/interstitial cystitis with botulinum toxin A: why isn't it effective in all patients? Transl. Androl. Urol. 4 (5), 543–554.
Lee, W.H., Shin, T.J., Kim, H.J., Lee, J.K., Suh, H.W., Lee, S.C., Seo, K., 2011. Intrathecal administration of botulinum neurotoxin type A attenuates formalin-induced antinociceptive responses in mice. Anesth. Analg. 112 (1), 228–235.
Lin, Y.Y., Tseng, T.J., Hsieh, Y.L., Luo, K.R., Lin, W.M., Chiang, H., Hsieh, S.T., 2008. Depletion of peptidergic innervation in the gastric mucosa of streptozotocin-induced diabetic rats. Exp. Neurol. 213 (2), 388–396.
Lindsay, R.M., Harmar, A.J., 1989. Nerve growth factor regulates expression of neuropeptide genes in adult sensory neurons. Nature 337, 362–364.
Luo, J., Feng, J., Liu, S., Walters, E.T., Hu, H., 2015. Molecular and cellular mechanisms that initiate pain and itch. Cell. Mol. Life Sci. 72 (17), 3201–3223.
Mathis, D., Vence, L., Benoist, C., 2001. Beta-Cell death during progression to diabetes. Nature 414 (6865), 792–798.
Meng, J., Wang, J., Steinhoff, M., Dolly, J.O., 2016. TNFα induces co-trafficking of TRPV1/TRPA1 in VAMP1-containing vesicles to the plasmalemma via Munc18-1/syntaxin1/SNAP-25 mediated fusion. Sci. Rep. 6, 21226.
Myers, M.I., Peltier, A.C., Li, J., 2013. Evaluating dermal myelinated nerve fibers in skin biopsy. Muscle Nerve 47 (1), 1–11.
Obrosova, I.G., 2009. Diabetes and the peripheral nerve. Biochim. Biophys. Acta 1792 (10), 931–940.
Osikowicz, M., Longo, G., Allard, S., Cuello, A.C., Ribeiro-da-Silva, A., 2013. Inhibition of endogenous NGF degradation induces mechanical allodynia and thermal hyperalgesia in rats. Mol. Pain 9, 37.
Pabbidi, R.M., Yu, S.Q., Peng, S., Khardori, R., Pauza, M.E., Premkumar, L.S., 2008. Influence of TRPV1 on diabetes-induced alterations in thermal pain sensitivity. Mol. Pain 4, 9.
Park, J., Park, H.J., 2017. Botulinum Toxin for the treatment of neuropathic pain. Toxins (Basel) 9 (9) pii: E260.
Paterson, K., Lolignier, S., Wood, J.N., McMahon, S.B., Bennett, D.L., 2014. Botulinum toxin-A treatment reduces human mechanical pain sensitivity and mechanotransduction. Ann. Neurol. 75 (4), 591–596.
Pezet, S., Malcangio, M., Lever, I.J., Perkinton, M.S., Thompson, S.W., Williams, R.J., McMahon, S.B., 2002. Noxious stimulation induces Trk receptor and downstream ERK phosphorylation in spinal dorsal horn. Mol. Cell. Neurosci. 21 (4), 684–695.
Pinho-Ribeiro, F.A., Verri Jr, W.A., Chiu, I.M., 2017. Nociceptor sensory neuron-immune interactions in pain and inflammation. Trends Immunol. 38 (1), 5–19.
Polydefkis, M., Hauer, P., Griffin, J.W., McArthur, J.C., 2001. Skin biopsy as a tool to assess distal small fiber innervation in diabetic neuropathy. Diabetes Technol. Ther. 3 (1), 23–28.
Provitera, V., Nolano, M., Pagano, A., Caporaso, G., Stancanelli, A., Santoro, L., 2007. Myelinated nerve endings in human skin. Muscle Nerve 35 (6), 767–775.
Purves, T., Middlemas, A., Agthong, S., Jude, E.B., Boulton, A.J., Fernyhough, P., Tomlinson, D.R., 2001. A role for mitogen-activated protein kinases in the etiology of diabetic neuropathy. FASEB J. 15 (13), 2508–2514.
Romanovsky, D., Cruz, N.F., Dienel, G.A., Dobretsov, M., 2006. Mechanical hyperalgesia correlates with insulin deficiency in normoglycemic streptozotocin-treated rats. Neurobiol. Dis. 24 (2), 384–394.
Samur, D.N., Arslan, R., Aydın, S., Bektas, N., 2018. Valnoctamide: the effect on relieving of neuropathic pain and possible mechanisms. Eur. J. Pharmacol. 827, 208–214.
Sandkühler, J., 2007. Understanding LTP in pain pathways. Mol. Pain 3, 9.
Shun, C.T., Chang, Y.C., Wu, H.P., Hsieh, S.C., Lin, W.M., Lin, Y.H., Tai, T.Y., Hsieh, S.T., 2004. Skin denervation in type 2 diabetes: correlations with diabetic duration and functional impairments. Brain 127 (Pt 7), 1593–1605.
Srebro, D., Vučković, S., Prostran, M., 2016. Participation of peripheral TRPV1, TRPV4, TRPA1 and ASIC in a magnesium sulfate-induced local pain model in rat. Neuroscience 339, 1–11.
Sumner, C.J., Sheth, S., Griffin, J.W., Cornblath, D.R., Polydefkis, M., 2003. The spectrum of neuropathy in diabetes and impaired glucose tolerance. Neurology 60 (1), 108–111.
Todorovic, S.M., 2016. Painful diabetic neuropathy: prevention or suppression? Int. Neuroscientist 127, 211–225.
Tripathi, B.K., Srivastava, A.K., 2006. Diabetes mellitus: complications and therapeutics. Med. Sci. Monit. 12 (7), RA130–RA147.
Umapathi, T., Tan, W.L., Loke, S.C., Soon, P.C., Tavintharan, S., Chan, Y.H., 2007. Intraepidermal nerve fiber density as a marker of early diabetic neuropathy. Muscle Nerve 35 (5), 591–598.
Wang, X.M., Lehky, T.J., 2012. Discovering cytokines as targets for chemotherapy-induced painful peripheral neuropathy. Cytokine 59 (1), 3–9.
Wood, K.W., Sarnecki, C., Roberts, T.M., Blenis, J., 1992. Ras mediates nerve growth factor receptor modulation of three signal-transducing protein kinases: MAP kinase, Raf- 1, and RSK. Cell 68 (6), 1041–1050.
Yasuda, H., Terada, M., Maeda, K., Kogawa, S., Sanada, M., Haneda, M., Kashiwagi, A., Kikkawa, R., 2003. Diabetic neuropathy and nerve regeneration. Prog. Neurobiol. 69 (4), 229–285.
Yuan, R.Y., Sheu, J.J., Yu, J.M., Chen, W.T., Tseng, I.J., Change, H.H., Hu, C.J., 2009. Botulinum toxin for diabetic neuropathic pain: a randomized double-blind crossover trial. Neurology 72 (17), 1473–1478.
Zhang, X., Chen, W.W., Huang, W.J., 2017. Chemotherapy-induced peripheral neuropathy. Biomed. Rep. 6 (3), 267–271.
Zhao, B., Wang, H.B., Lu, Y.J., Hu, J.W., Bao, L., Zhang, X., 2011. Transport of receptors, receptor signaling complexes and ion channels via neuropeptide-secretory vesicles. Cell Res. 21 (5), 741–753.
Zhuang, Z.Y., Xu, H., Clapham, D.E., Ji, R.R., 2004. Phosphatidylinositol 3-kinase activates ERK in primary sensory neurons and mediates inflammatory heat hyperalgesia through TRPV1 sensitization. J. Neurosci. 24 (38), 8300–8309.